Arginine metabolism, polyamine homeostasis and ferroptosis in cancer: Molecular links and therapeutic opportunities (Review)

XIN DONG[1,2*], YONGKUN HOU[1,2*], JINGJING SHAO[3], HAIXIA ZHU[3] and JIBIN LIU[4]

[1]School of Medicine, Nantong University, Nantong, Jiangsu 226019, P.R. China; [2]Affiliated Tumor Hospital of Nantong University, Nantong, Jiangsu 226361, P.R. China; [3]Cancer Research Center Nantong, Affiliated Tumor Hospital of Nantong University and Nantong Tumor Hospital, Nantong, Jiangsu 226361, P.R. China; [4]Institute of Oncology, Affiliated Tumor Hospital of Nantong University, Nantong, Jiangsu 226361, P.R. China

Received June 5, 2026; Accepted August 17, 2026

DOI: 10.3892/mmr.2026.14022

Abstract. Arginine metabolism, polyamine homeostasis and ferroptosis are interconnected molecular processes that influence tumor growth, immune remodeling and therapeutic responses. The availability of arginine is affected by tumor-cell biosynthesis and uptake, myeloid arginase (ARG)-mediated depletion, nitric oxide synthase (NOS)-driven diversion and stromal-vascular nutrient transport and microenvironmental remodeling. These input signals regulate the synthesis, uptake-efflux cycling and catabolic turnover of polyamines, thereby creating an inhibitory buffering state or an oxidative state that can lower the ferroptosis threshold. Ferroptosis is controlled by the balance of lipid peroxidation triggers, including polyunsaturated fatty acid-phospholipid load, iron-dependent amplification and lipoxygenase activity, as well as buffering systems such as the cystine/glutamate antiporter system Xc^--glutathione-glutathione peroxidase 4 axis, ferroptosis suppressor protein 1-coenzyme Q10, dihydroorotate dehydrogenase and GTP cyclohydrolase 1-tetrahydrobiopterin (BH4). The immunological consequences of ferroptotic tumor-cell death are context-dependent, as dying cells may promote interferon-gamma-driven antitumor immunity or, conversely, reinforce myeloid-mediated immunosuppression. The present review summarized the molecular links among arginine metabolism, polyamine homeostasis and ferroptosis in cancer and discusses therapeutic opportunities involving biomarker-guided combinations targeting arginine, polyamine blockade, ferroptosis sensitization and immune checkpoint blockade.

Correspondence to: Dr Haixia Zhu, Cancer Research Center Nantong, Affiliated Tumor Hospital of Nantong University and Nantong Tumor Hospital, 30 Tongyang North Road, Nantong, Jiangsu 226361, P.R. China
E-mail: 00zlingling@163.com

Dr Jibin Liu, Institute of Oncology, Affiliated Tumor Hospital of Nantong University, 30 Tongyang North Road, Nantong, Jiangsu 226361, P.R. China
E-mail: tians2008@ntu.edu.cn

*Contributed equally

Abbreviations: ASS1, argininosuccinate synthase 1; ARG, arginase; CAF, cancer-associated fibroblast; DFMO, difluoromethylornithine; DHODH, dihydroorotate dehydrogenase; FSP1, ferroptosis suppressor protein 1; GCH1, GTP cyclohydrolase 1; GPX4, glutathione peroxidase 4; GSH, glutathione; ICB, immune checkpoint blockade; NOS, nitric oxide synthase; PAOX, polyamine oxidase; ROS, reactive oxygen species; SAT1, spermidine/spermine N1-acetyltransferase 1; SMOX, spermine oxidase; TME, tumor microenvironment

Key words: arginine metabolism, polyamine homeostasis, ferroptosis, tumor microenvironment, lipid peroxidation; immunometabolism, immune checkpoint blockade, therapeutic opportunities

Contents

1. Introduction

Over the past five years, research on cancer immunometabolism has shifted from characterizing isolated metabolic abnormalities to establishing nutrient availability as a dynamic determinant of immune-cell fitness and therapeutic responses. Arginine has become a core regulatory node, as its local availability is jointly controlled by tumor-cell biosynthesis and uptake, arginase 1 (ARG1)/arginase 2 (ARG2) activity,

nitric oxide synthase (NOS)-dependent metabolic diversion and stromal-vascular transport. Experimentally, using engineered bacteria to increase intratumoral L-arginine enhanced T-cell infiltration and produced a synergistic effect with programmed death-ligand 1 (PD-L1) blockade, while low-arginine conditions trigger metabolic and transcriptional reprogramming in activated $CD4^+$ T cells via the activating transcription factor 4 (ATF4)-solute carrier family 7 member 11 (SLC7A11)-GSH axis, ultimately endowing T cells with Treg-like immunosuppressive properties (1,2).

Meanwhile, studies have linked arginine-derived polyamine metabolism to ferroptosis and immune remodeling. Arginine-derived polyamines can enhance ferroptosis through H_2O_2-dependent lipid peroxidation and an iron overload-WNT/MYC proto-oncogene (MYC)-ornithine decarboxylase 1 (ODC1)-polyamine positive-feedback circuit (3). However, ferroptosis is not uniformly immunostimulatory. Ferroptotic cancer cells may impair dendritic-cell maturation and antigen cross-presentation and the immunological consequences of ferroptosis vary depending on the affected cell populations, the stage of cell death and the surrounding microenvironment (4,5). These advances reveal major unresolved issues: Arginine metabolism, polyamine homeostasis, ferroptosis susceptibility and immune feedback are still generally regarded as independent processes and static measurements of individual enzymes or metabolites cannot adequately explain the differential responses among spatially heterogeneous tumors. Therefore, a comprehensive framework is required to connect these processes with biomarker-guided patient stratification and rational treatment sequences.

In this context, two recurring challenges remain. First, explanations based on single pathways are insufficient to account for why the same metabolic perturbation can produce different or even opposite immune outcomes in different tumor types and spatial microenvironments. Second, although a number of individual mechanisms are biologically plausible, the field still lacks a transferable framework that connects metabolic states with pharmacological interventions, treatment sequences and biomarker-guided patient stratification.

To address these challenges, the present study conceptualized the tumor microenvironment (TME) as a state-matched immunopharmacology system organized around four interrelated layers, as illustrated in Fig. 1. The Input layer includes the availability of extracellular arginine and its local regulation through biosynthesis, membrane transport, ARG1/ARG2-mediated depletion and NOS-dependent metabolic diversion, thereby defining the nutritional and metabolic pressures imposed on tumor and immune cells. The State layer describes how these upstream inputs are redistributed through the synthesis of ornithine and polyamines, the uptake-efflux cycling, polyamine catabolism and antioxidant buffering, collectively establishing a polyamine-dominated suppressive state or an oxidative state approaching the ferroptosis threshold. The Output layer represents the executable biological phenotypes generated by these metabolic states, including tumor-cell survival or ferroptosis, as well as the preservation or impairment of effector T-cell function. The Feedback layer captures how tumor-cell death, interferon-γ (IFN-γ) signaling, antigen presentation and myeloid remodeling subsequently reshape arginine consumption, redox defenses and therapeutic sensitivity.

From this perspective, the key question is not merely whether a particular marker is increased or decreased, but whether the therapeutic intervention aligns with the relevant functional thresholds, such as the effector T-cell functional threshold or the ferroptosis execution threshold. Equally important is whether the output of resulting tumor-cell death translates into enhanced antitumor immunity or is redirected toward suppressive immune remodeling. Together, these four layers provide the primary organizational logic for the subsequent sections.

2. The arginine niche as an immunometabolic input for pharmacological intervention

Defining the niche: Supply-side processes of biosynthesis, uptake and recycling. The core of the arginine niche concept lies in transcending the view of 'arginine availability' as a single concentration-based indicator, instead defining it as a system-level balance of local exchangeable flux. Within any given tumor microdomain, the net availability of arginine is determined by the relative strengths of two sets of processes. The first set consists of supply-side processes that determine how arginine enters cells or the local exchangeable pool. These processes include compensatory biosynthesis, transmembrane uptake and recycling within tumor cells, as well as processes in selected stromal or immune-cell populations. The second set comprises demand-side processes that drive the consumption of arginine or its conversion into chemical stress-inducing mediators. These processes include myeloid-dominated depletion through ARG1/ARG2 and NOS-driven diversion through the NOS-nitric oxide (NO)/reactive nitrogen species (RNS) axis (6-9).

This supply-demand framework is important because it establishes strict consistency requirements for subsequent sections. Any discussion regarding polyamine homeostasis or ferroptosis thresholds must first define the upstream arginine background in a given microdomain: Whether the state is primarily driven by supply deficiency, excessive consumption, or the superimposition of both processes (7-9).

This control node is intrinsically spatially heterogeneous. Within the same tumor tissue, different microdomain states may coexist, such as regions with limited supply but moderate consumption, or regions with relatively preserved supply but strong consumption pressure. These heterogeneous microdomains may exert different or even opposing regulatory effects on the polyamine homeostasis at the State layer and the ferroptosis threshold at the Output layer, leading to different biological predictions. This spatially resolved interpretation provides a conceptual basis for the subsequent development of state-based tumor stratification strategies (6-11).

Tumor-cell compartment: biosynthesis-dependent axis and transport competition involving argininosuccinate synthase 1 (ASS1)/argininosuccinate lyase (ASL) and cationic amino acid transporters (CATs). To avoid simplifying arginine regulation to a mere upregulation or downregulation of a single gene, the present study described the arginine handling in tumor cells as a biosynthesis-dependent axis. One end of this axis represents a relatively self-sufficient state, where tumor cells maintain effective arginine replenishment through

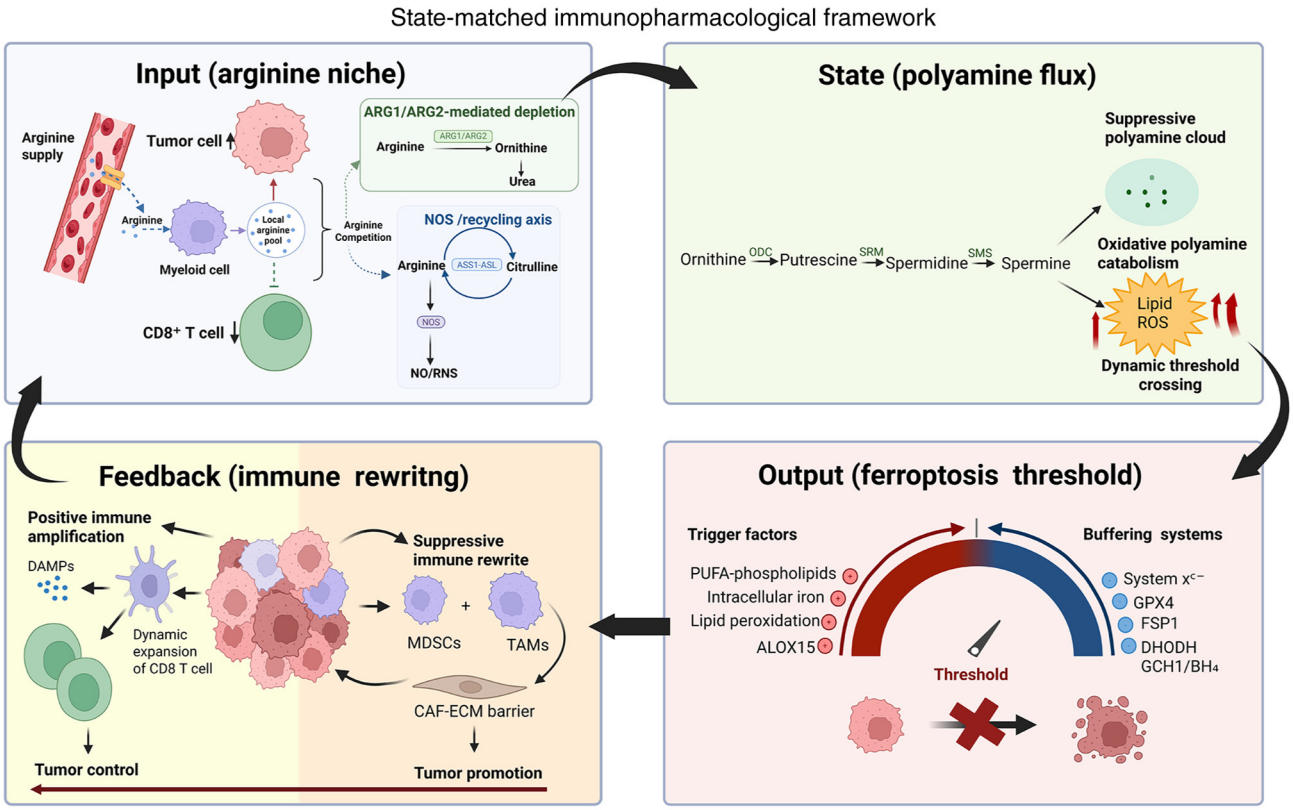

Figure 1. State-matched immunopharmacological framework integrating the arginine niche, polyamine flux, ferroptosis threshold and immune feedback. The arginine niche acts as the Input layer, polyamine flux as the State layer, ferroptosis threshold as the therapeutic output and immune rewiring as the Feedback layer. ARG1, arginase 1; ARG2, arginase 2; NOS, nitric oxide synthase; NO/RNS, nitric oxide/reactive nitrogen species; CD8, cluster of differentiation 8; ASS1, argininosuccinate synthase 1; ASL, argininosuccinate lyase; ODC, ornithine decarboxylase; SRM, spermidine synthase; SMS, spermine synthase; ROS, reactive oxygen species; DAMPs, damage-associated molecular patterns; MDSCs, myeloid-derived suppressor cells; TAMs, tumor-associated macrophages; CAF, cancer-associated fibroblast; ECM, extracellular matrix; PUFA, polyunsaturated fatty acid; ALOX15, arachidonate 15-lipoxygenase; system x_c^-, cystine/glutamate antiporter; GPX4, glutathione peroxidase 4; FSP1, ferroptosis suppressor protein 1; DHODH, dihydroorotate dehydrogenase; GCH1, GTP cyclohydrolase 1; BH_4, tetrahydrobiopterin.

endogenous synthesis or citrulline-to-arginine recycling. The other end represents an auxotrophic state, where the replenishment capacity of tumor cells is limited and highly dependent on exogenous arginine (12,13). This axis constitutes the core coordinates of the Input layer, as it not only determines whether tumor cells are susceptible to extracellular arginine-deprivation strategies but also dictates their competitive intensity for local arginine against immune cells in the TME. When tumor cells lack sufficient endogenous arginine self-sufficiency, they may compensate by enhancing arginine uptake and recycling programs. This adaptive response shifts the niche-level competitive pressure onto immune cells, reducing the residual arginine flux available to effector T cells, thereby pushing these cells below the functional threshold required for activation, proliferation and cytotoxicity (14,15).

At the molecular level, compensatory arginine biosynthesis is primarily mediated by ASS1 and ASL, which cooperate to recycle citrulline back into arginine and establish a buffering loop to cope with fluctuations in extracellular arginine availability (16). In parallel, CATs, particularly context-dependent members of the solute carrier family 7 (SLC7), support the uptake of extracellular arginine, thereby determining the efficiency with which tumor cells utilize the local exchangeable arginine pool. The ASS1/ASL-dependent recycling and CAT-mediated uptake together determine whether tumor cells act as replenishment-competent competitors or arginine-dependent consumers within the niche.

However, in multiple types of tumors, ASS1 may be epigenetically silenced or transcriptionally suppressed. This change should not be interpreted merely as an incidental metabolic defect; in some cases, it represents an adaptive response to metabolic pressure in the TME. The inhibition of ASS1 may be related to metabolic redistribution between the urea cycle and *de novo* pyrimidine synthesis, increasing dependence on extracellular arginine and providing a selective growth advantage under specific nutritional conditions (17-19). In this context, CAT-mediated uptake becomes particularly important, as the loss of endogenous replenishment increases reliance on the extracellular arginine pool. Thus, tumors with low ASS1 expression may become vulnerable to arginine deprivation treatment while imposing stronger arginine competition on infiltrating immune cells.

More importantly, these biosynthetic and transport processes often collaborate with stress-responses and oncogenic pathways, including the integrated stress response/ATF4 axis, MYC- or KRAS proto-oncogene, GTPase (KRAS)-driven metabolic reprogramming and stromal constraints. These interactions can form a self-reinforcing adaptive chain: insufficient arginine replenishment enhances dependence on transporter-mediated uptake and recycling processes; increased

consumption by tumor cells reduces immune-accessible arginine flux below the functional threshold for effector T cells; and the resulting immunosuppressive microenvironment further supports tumor-cell survival in areas of inadequate perfusion or spatial constraints (20,21). Therefore, before discussing polyamine homeostasis or ferroptosis thresholds, it is necessary to define the position of a given tumor state on this axis: a state of sufficient replenishment and relative self-sufficiency, or a dependence-driven, competition-dominated state. These two configurations imply fundamentally different pharmacological vulnerabilities and combination treatment strategies.

Myeloid compartment: ARG1/ARG2-mediated depletion and T-cell threshold crossing. In a number of solid tumors, the dominant regulators of the L-arginine niche are not necessarily the tumor cells themselves, but myeloid populations, including myeloid-derived suppressor cells (MDSCs), tumor-associated macrophages (TAMs) and tumor-associated neutrophils (TANs). These compartments converge on a common functional endpoint, reducing the extracellular arginine pool and impairing T-cell activity, but differ in their developmental state, tissue localization, deployment of ARG and accompanying suppressive mediators. Therefore, MDSCs, TAMs and TANs should not be viewed as interchangeable sources of ARG activity. MDSCs represent a heterogeneous population, including polymorphonuclear MDSCs (PMN-MDSCs) and monocytic MDSCs (M-MDSCs). PMN-MDSCs typically couple arginine depletion dependent on ARG1 with the generation of reactive oxygen species (ROS) or peroxynitrite produced by nicotinamide adenine dinucleotide phosphate (NADPH) oxidase 2 (NOX2), while M-MDSCs more frequently utilize NO dependent on nitric oxide synthase 2 (NOS2) and context-dependent suppressive cytokines. These distinctions are not absolute, as the TME can functionally reprogram these myeloid subsets. In particular, hypoxia and hypoxia-inducible factor 1 alpha (HIF-1α) signaling can increase the expression of ARG1 and NOS2, expanding the suppressive activity of tumor-infiltrating MDSCs and promoting their differentiation into macrophage-like states (22,23). Therefore, MDSCs serve as a plastic suppressive compartment, where arginine depletion is combined with oxidative, nitrosative and cytokine-mediated inhibition (22,23). TAMs represent a more differentiated and spatially persistent myeloid compartment. In the suppressive TAM state, ARG1-mediated arginine hydrolysis not only limits the substrate available to infiltrating T cells but also increases the availability of ornithine for downstream polyamine synthesis and tissue-remodeling pathways (24). Importantly, ARG1 should not be viewed solely as a marker of macrophage polarization. In pancreatic cancer models, macrophage-specific Arg1 deletion delayed the development of aggressive tumors and increased the infiltration of $CD8^+$ T cells, while pharmacological ARG inhibition further enhanced tumor sensitivity to programmed cell death protein 1 (PD-1) blockade (24). Arg1 deletion also induced compensatory Arg2 expression in a subset of macrophages, indicating that mitochondrial ARG2 may serve as a context-dependent intracellular adaptive pathway rather than a unified extracellular depletion mechanism for all myeloid cells (24). TANs and PMN-MDSCs share similarities in morphological and functional characteristics, and the distinctions between these populations may become blurred within tumors (22,25). A characteristic of human neutrophils is the storage of ARG1 in intracellular granules. Upon activation and degranulation, ARG1 can be released into the extracellular space, where it rapidly consumes local L-arginine and inhibits T-cell proliferation. This release-based mechanism differs from the more persistent transcriptional and metabolic programs observed in TAMs and provides a rapid pathway for neutrophil-rich tumor regions to establish local arginine deprivation (25). However, not every tumor-infiltrating neutrophil is immunosuppressive; therefore, the functional identification of TANs or PMN-MDSCs relies on their immunosuppressive activity and metabolic profiles, rather than solely on granulocytic phenotypic markers.

Despite these differences, all three compartments can cooperate to maintain a low-flux arginine niche. MDSCs provide a flexible combination of ARG, ROS, RNS and cytokine-dependent suppression; TAMs establish sustained tissue-resident metabolic and polyamine-remodeling programs, while TANs can rapidly release extracellular ARG1 through degranulation. Their common downstream effects include reduced expression of the T-cell receptor CD3ζ, impaired proliferation and decreased production of cytokines and cytotoxic effectors. Therefore, distinguishing these cell origins is important for biomarker selection and determining whether ARG inhibition should be combined with MDSC-directed, macrophage-directed or neutrophil-directed interventions.

This depletion has significant immunological consequences, as T-cell function is highly dependent on the availability of arginine. When local arginine flux falls below the functional threshold required for effector T-cell activation, proliferation and cytotoxicity, the effector program may experience a switch-like collapse. This collapse is characterized by impaired clonal expansion, reduced production of cytotoxic molecules and cytokines and a shift in metabolic and signaling programs toward a maintenance state or dysfunctional state (26,27). Therefore, the ecological effects of the myeloid ARG axis are threshold-amplifying. It does not require uniformly high ARG expression throughout the entire tumor mass. Sustained arginine depletion in selected microdomains, such as regions distant from blood vessels, regions behind cancer-associated fibroblast (CAF)-extracellular matrix (ECM) barriers, or peri-necrotic zones, may be sufficient to push local immunity below the execution threshold and establish a suppressive state where immune-mediated tumor clearance becomes inefficient (28).

This connection links the Input layer, represented by the arginine niche, to the State layer, represented by polyamine homeostasis. A stronger ARG axis increases the conversion of arginine to ornithine, thereby expanding the precursor supply for polyamine biosynthesis and favoring a state characterized by high polyamine flux and stabilized immunosuppression. Under specific stress conditions, the involvement of the polyamine catabolic axis may further reshape this state. The catabolism mediated by polyamine oxidase (PAOX) and spermine oxidase (SMOX) can generate ROS, including H_2O_2, thereby increasing lipid-peroxidation pressure and weakening residual anti-ferroptotic buffering capacity. This may create a therapeutic window in which ARG inhibition, polyamine

blockade, ferroptosis sensitization and ICB can be rationally combined. In this sense, the myeloid ARG axis is not an auxiliary mechanism but a key bridge that transmits the arginine depletion of the Input layer to downstream state remodeling and the output-layer's ferroptosis vulnerability (29-31).

Diversion axis: NOS-NO/RNS converts nutrient limitation into oxidative and nitrosative chemical stress. If ARG1/ARG2-mediated depletion primarily suppresses antitumor immunity by depleting the local exchangeable arginine pool below the functional threshold required for effector T-cell activity, then NOS-mediated arginine diversion represents a form of chemical amplification of niche perturbation. It not only consumes arginine but also converts this substrate into diffusible stress mediators, including NO and downstream RNS. Therefore, the diversion axis should not be viewed merely as another mode of arginine consumption. Instead, it transforms nutritional limitation from a substrate supply issue into a broader chemical stress state within the TME.

Under comparable conditions of reduced local arginine, a diversion-dominant niche imposes an additional NO/RNS-driven oxidative and nitrosative baseline. This baseline can suppress immune execution, reset redox homeostasis and increase lipid-peroxidation pressure, thereby preconditioning the system for subsequent changes in the threshold of ferroptosis (32,33). In this sense, NOS-mediated diversion not only links the Input layer to T-cell functional impairment but also associates with downstream redox remodeling and susceptibility to ferroptosis.

The clinical significance of NOS-mediated diversion lies not merely in the simple suppression or enhancement of NO production, but in identifying the flux- and context-dependent switches that determine its biological output. In MCF7 cells under defined aerobic conditions, low steady-state NO concentrations (<50 nM) activate extracellular signal-regulated kinase (ERK) through soluble guanylate cyclase, moderate concentrations (>100 nM) promote the accumulation of HIF-1α, while higher concentrations (>300 nM) induce p53 Ser15 phosphorylation. These values should not be interpreted as universal clinical cutoffs. Instead, they provide experimental evidence that NO concentration and exposure time can participate in different signaling programs, while oxygen consumption, cell density and ROS production can alter effective thresholds (34).

In immune-cold or myeloid-dominated microenvironments, the balance between NO and superoxide acts as a critical molecular switch. M-MDSCs predominantly suppress T-cell responses through inducible nitric oxide synthase (iNOS)-derived NO, whereas granulocytic MDSCs can generate peroxynitrite through the simultaneous production of NO and superoxide. Experimental inhibition of iNOS-derived NO preferentially impairs monocytic MDSC-mediated suppression, while the clearance of peroxynitrite or the disruption of endothelial nitric oxide synthase (eNOS)- and NOX2-dependent oxidant production reduces the suppressive activity of granulocyte MDSCs (22). Thus, NO-dominant and peroxynitrite-dominant tumor niches induce T-cell dysfunction via different chemical mechanisms.

The regulatory relationship between NO signaling and ferroptosis is bidirectional and context-dependent. In activated macrophages, iNOS-derived NO can inhibit the generation of ferroptotic phospholipid signals. Genetic or pharmacological inhibition of iNOS renders M1 macrophages sensitive to GPX4-inhibitor-induced ferroptosis, while NO donors increase the ferroptosis resistance of M2 macrophages. This protective effect is related to the nitroxidative interference with 15-lipoxygenase-dependent phospholipid oxidation and oxidized phosphatidylethanolamine (PE) intermediates (35).

Conversely, when NO and superoxide are co-generated in an iron-rich environment with weakened GSH-GPX4 buffering, the formation of peroxynitrite can increase lipid-peroxidation pressure and facilitate ferroptosis. In an engineered NO-generating tumor model, the production of NO promoted GSH consumption, reduced GPX4 expression, increased heme oxygenase 1-associated Fe^{2+} release and enhanced lipid peroxidation (36). This evidence should be interpreted as a context-dependent pro-ferroptotic configuration rather than as a universal property of NO. Therefore, the functional consequences of the axis shift depend on NO concentration and exposure time, the NO-to-superoxide balance, cellular identity, oxygen tension, labile iron availability and the capacity of GPX4-dependent and GPX4-independent antioxidant systems. These variables determine whether NOS-NO/RNS signaling primarily suppresses immune execution, protects specific myeloid cells from ferroptosis or facilitates ferroptosis in tumor-cell death.

Stromal and vascular compartments: Spatial barriers as amplifiers of arginine depletion. The arginine niche should be viewed as a niche, not just a metabolic pathway, because its determining factors are not limited to the intrinsic activity of metabolic enzymes. They also include the spatial organization of transport, perfusion and diffusion. In most solid tumors, abnormal vasculature, heterogeneous perfusion, elevated interstitial pressure and dense CAF-ECM matrix collectively create a geographically constrained supply environment. Once nutrients diffuse out of the vasculature into tumor tissues, their effective diffusion range is markedly restricted. Therefore, microdomains located far from functional blood vessels may be chronically exposed to low-flux arginine states.

Under these conditions, myeloid ARG-mediated depletion or NOS-driven diversion are amplified, not necessarily because the enzymatic activity in these regions is higher, but because the replenishment of arginine is more difficult to deliver. Slower delivery kinetics, elongated diffusion trajectories and stromal barriers transform transient local nutrient depletion into persistent substrate scarcity (37-40). In this sense, the stromal and vascular compartments act as depletion amplifiers. They stabilize transient arginine consumption into spatially fixed low-arginine microdomains, increasing the likelihood of impaired T-cell function. Therefore, the inhibitory consequences of arginine limitation cannot be fully understood without considering the physical context embedded in nutrient delivery, cellular consumption and metabolic competition.

The essence of a low-perfusion region is input limitation. Even with normal plasma arginine levels, insufficient perfusion or vascular leakage can reduce effective local delivery, causing the exchangeable arginine pool within selected microdomains to remain at low levels (37-40). More importantly, the restricted supply and enhanced consumption do not simply

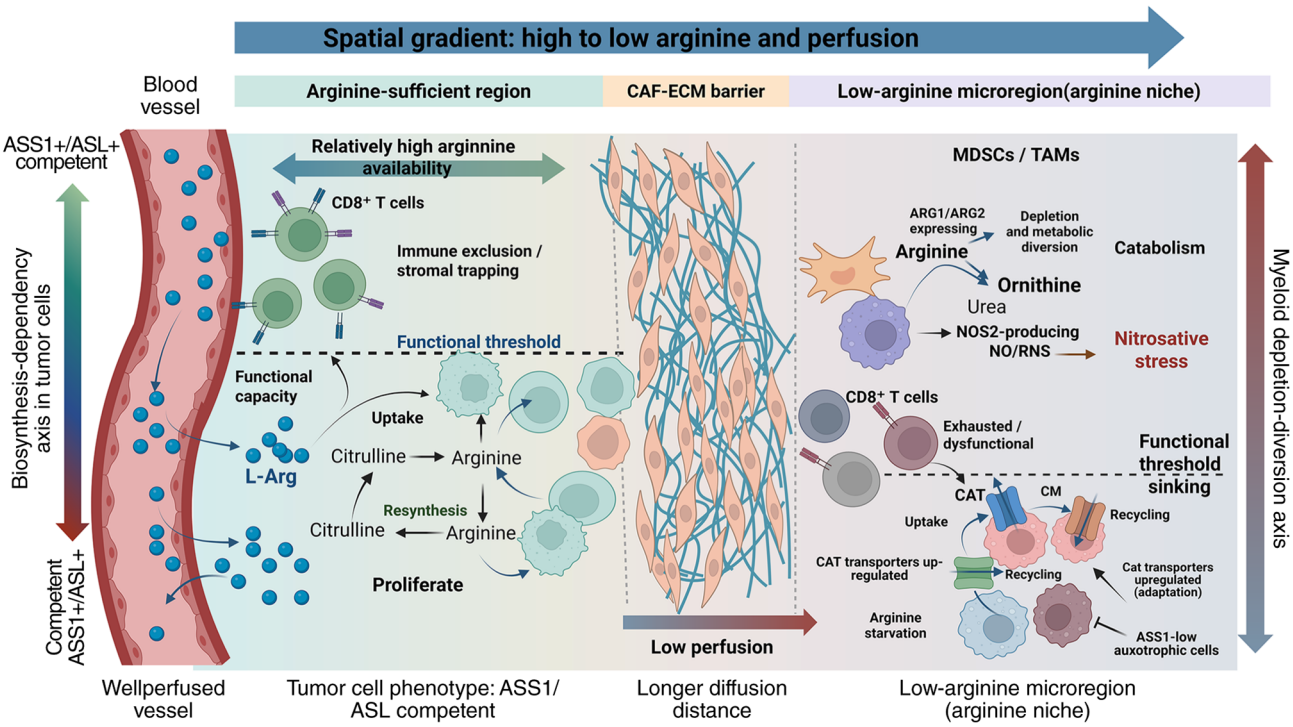

Figure 2. Spatial organization of the arginine niche. Vascular supply, ASS1/ASL-dependent biosynthesis, CAT-mediated uptake, ARG1/ARG2-mediated depletion, NOS-driven diversion and CAF-ECM barriers generate microdomain-specific arginine availability and immune functional thresholds. ASS1, argininosuccinate synthase 1; ASL, argininosuccinate lyase; ARG1, arginase 1; ARG2, arginase 2; CAF, cancer-associated fibroblast; CAT, cationic amino acid transporter; CM, cell membrane; ECM, extracellular matrix; CD8, cluster of differentiation 8; NOS2, nitric oxide synthase 2; NO/RNS, nitric oxide/reactive nitrogen species; L-Arg, L-arginine; MDSCs, myeloid-derived suppressor cells; TAMs, tumor-associated macrophages.

linearly add up. Instead, they are more likely to produce nonlinear amplification near functional thresholds. When abnormal perfusion and diffusion limitations reduce local arginine supply to near the critical requirements needed for effector T-cell activity, even slight additional ARG-mediated depletion or tumor-cell uptake competition may be sufficient to push local arginine flux below the threshold required for CD3ζ expression, cell-cycle progression and cytotoxic function (26,27,37-40). By contrast, in relatively well-perfused regions, the same degree of arginine consumption may only lead to partial inhibition, insufficient to trigger sustained T-cell functional inactivation (26,27,37-40).

Stromal and vascular compartments can also shape niche plasticity through changes in tissue architecture and perfusion (38,39). Therefore, structural interventions, such as stromal decompression or vascular normalization, should be understood as strategies to alter system boundary conditions. By increasing supply flux, shortening diffusion distances, and reducing the amplification factors of depletion, these interventions may restore the availability of local arginine above the functional threshold for effector T-cell activity and create space for subsequent combination therapies (38,39). Overall, the strength of the arginine niche is determined not only by metabolism but also by transport. In tumors characterized by low perfusion or a dense stromal matrix, transport bottlenecks act as a multiplicative factor, amplifying arginine depletion (37-40). The spatial organization of the arginine niche, including vascular supply, tumor-cell uptake, myeloid-mediated depletion, NOS-driven diversion and stromal barriers, is summarized in Fig. 2.

3. Polyamine flux as a targetable state variable

Polyamine metabolism represents a State layer through which arginine availability is translated into proliferative, immunosuppressive and redox-adaptive programs. In this framework, polyamine flux is viewed not only as a downstream product of arginine catabolism but also as a targetable state variable that determines whether the system remains in a suppressive buffering state or shifts towards oxidative stress and ferroptosis sensitivity.

As illustrated in Fig. 3, the buffering branch is maintained by ODC1- and adenosylmethionine decarboxylase 1 (AMD1)-dependent polyamine synthesis, as well as uptake and efflux cycling. This branch maintains the availability of polyamines, supports tumor-cell proliferation and stress tolerance, and reinforces the suppressive polyamine cloud. By contrast, the oxidative-triggered branch is mediated by spermidine/spermine N1-acetyltransferase 1 (SAT1)-mediated acetylation and back-conversion, PAOX-dependent oxidation of acetylated polyamines and SMOX-dependent oxidation of spermine. These catabolic pathways produce H_2O_2, aldehydes and carbonyl stress, thereby increasing lipid-peroxidation pressure and lowering the ferroptosis threshold. Thus, Fig. 3 distinguishes between polyamine retention and recycling that favors buffering and oxidative polyamine catabolism that may prepare Output layers for ferroptosis.

The synthetic axis: From arginine-derived ornithine to the ODC1-AMD1 program. The polyamine synthetic axis provides a direct pathway through which the arginine niche

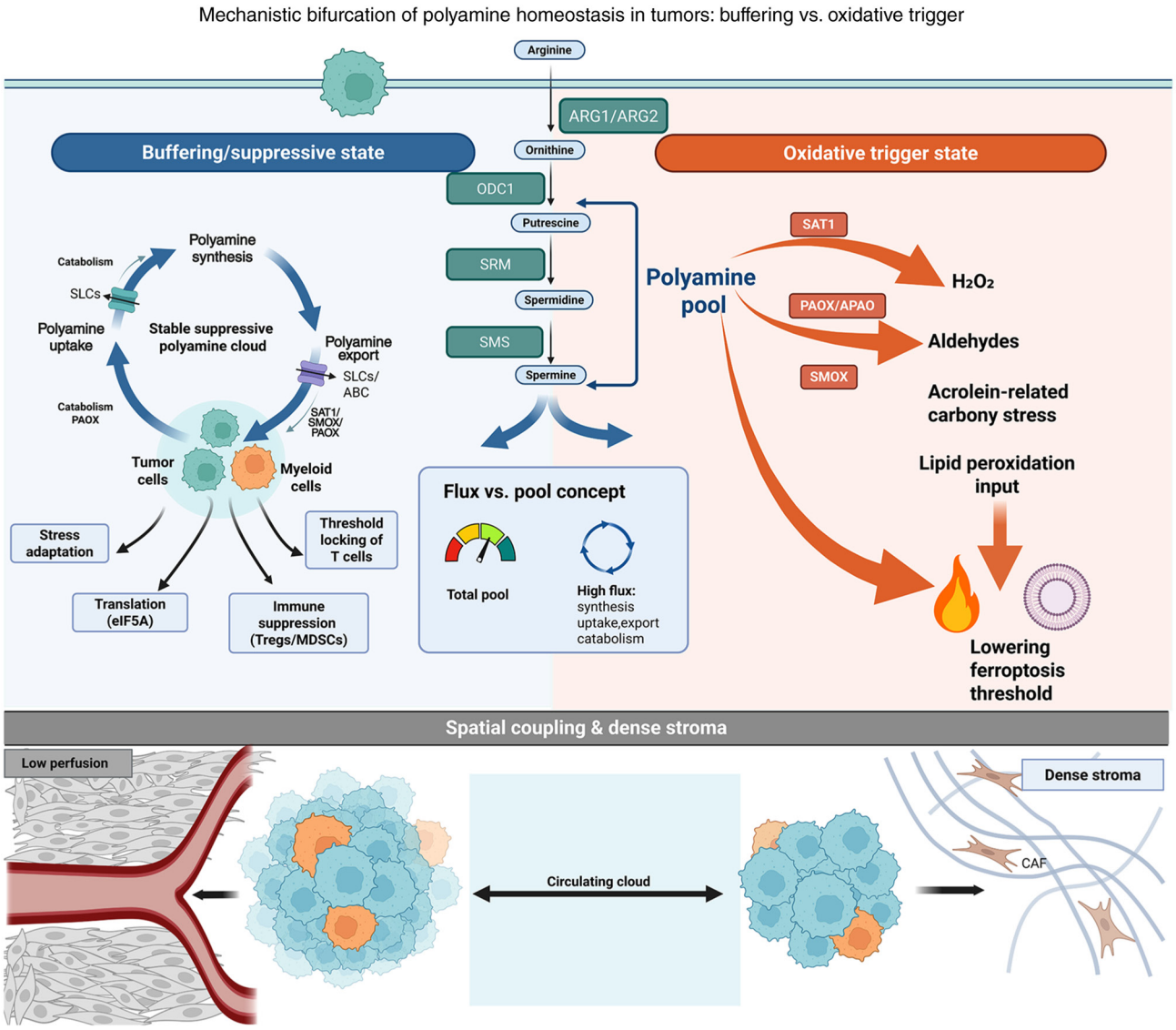

Figure 3. Mechanistic bifurcation of polyamine homeostasis. Polyamine synthesis and uptake-efflux cycling can stabilize a buffering or suppressive state, whereas SAT1-, PAOX- and SMOX-associated catabolism can generate H_2O_2, aldehydes and carbonyl stress that lower the ferroptosis threshold. SAT1, spermidine/spermine N1-acetyltransferase 1; PAOX, polyamine oxidase; APAO, acetylpolyamine oxidase; SMOX, spermine oxidase; ARG1, arginase 1; ARG2, arginase 2; ODC1, ornithine decarboxylase 1; SRM, spermidine synthase; SMS, spermine synthase; SLCs, solute carrier family transporters; ABC, ATP-binding cassette transporters; eIF5A, eukaryotic translation initiation factor 5A; Tregs, regulatory T cells; MDSCs, myeloid-derived suppressor cells; CAF, cancer-associated fibroblast; H_2O_2, hydrogen peroxide.

is converted into cellular states. Arginine is converted to ornithine via ARG1/ARG2, which is then decarboxylated by ODC1 to produce putrescine. Putrescine is further converted to spermidine and spermine through spermidine synthase (SRM)- and spermine synthase (SMS)-mediated aminopropyl-transfer reactions, while AMD1 generates decarboxylated S-adenosylmethionine, which is the required aminopropyl donor for maintaining this process (41).

The importance of this axis lies not only in the enzymatic reactions. Enhanced ARG-mediated arginine catabolism can channel substrates towards ornithine-dependent polyamine biosynthesis, thereby linking the arginine niche at the Input layer to polyamine homeostasis at the State layer. This connection can be summarized through three dimensions: Ornithine supply, ODC1-SRM-SMS-driven biosynthetic activity and AMD1-dependent aminopropyl-donor capacity. Together, these features determine whether the system enters a polyamine high-buffering state that supports tumor-cell proliferation, stress tolerance and immune suppression (30,41,42). The core state characteristics of the polyamine synthetic axis, including ornithine availability, synthetic driving force and methyl-donor restriction, are summarized in Table I.

Polyamine levels and polyamine flux: Why flux language is necessary. Polyamine homeostasis can only be treated as a central State-layer processor when defined by flux rather than static pool size. The total polyamine levels measured by metabolomics largely reflect cellular storage, as a number of intracellular polyamines are bound to nucleic acids, proteins or other macromolecular structures. Therefore, total abundance does not necessarily represent the exchangeable pool involved in signaling, stress adaptation, redox reactions or ferroptosis regulation. What determines immunosuppressive buffering and susceptibility for ferroptosis is not merely how much

Table I. Minimal state dimensions of the polyamine synthetic axis.

Core dimension	Variable composition	Biological significance
Ornithine supply	Intensity of ARG-mediated depletion/tumor metabolic phenotype	Determines the substrate basis for polyamine biosynthesis. High ARG activity or tumor metabolic reprogramming can provide sufficient precursors.
Synthetic driving capacity	ODC1-AMD1 activity axis	Determines the driving force and rate of polyamine biosynthesis. ODC1 represents the rate-limiting step, whereas AMD1 supports sustained progression of the synthetic chain.
Methyl-donor constraint	SAM/dcSAM balance	Determines the resource boundary of polyamine biosynthesis and its coupling with epigenetic regulation. The direction of this balance shapes the interaction between metabolism and epigenetic state.

AMD1, adenosylmethionine decarboxylase 1; ARG, arginase; ODC1, ornithine decarboxylase 1; SAM, S-adenosylmethionine; dcSAM, decarboxylated S-adenosylmethionine.

polyamine is stored, but how polyamines are synthesized, imported, exported and catabolized (42-45).

This flux-based perspective can be summarized through three operational dimensions: Synthetic drive, reflected by ODC1/AMD1/SRM/SMS activity and ornithine supply; state externalization, reflected by acetylated polyamines that indicate readiness for efflux or catabolic entry; and oxidative input, reflected by SAT1/PAOX/SMOX-associated catabolism, which redirects the polyamine pools toward ROS-generating flux. Methodologically, using labeled arginine or ornithine for stable isotope tracing can directly estimate the flux of polyamine biosynthesis. In more clinically accessible settings, acetylated-to-total polyamine ratios, combined with the characteristics of synthetic and catabolic genes, may serve as a practical alternative readout. These readouts should be interpreted alongside spatial features such as hypoxia, low perfusion and myeloid enrichment, aligning polyamine state variables with the actual architecture of the TME (32,33).

Uptake-efflux cycling: Polyamines as a diffusible 'polyamine cloud'. Once polyamine homeostasis is defined as a flux-based state rather than a static pool, uptake-efflux cycling becomes a key determinant of whether polyamine metabolism acts solely within individual cells or extends to tissue scale. Intercellular transfer allows polyamines to shape the microenvironment beyond their synthesizing cells, thereby linking intracellular metabolic states with population-level immune and redox regulation (46).

The present review defined the spatially persistent, polyamine-rich inhibitory environment maintained by uptake, efflux and local retention as the polyamine cloud. This concept refers not merely to an increase in polyamine abundance at a given time point. Instead, it describes a continuous background flux state that relies on ongoing polyamine exchange and is particularly relevant in low-perfusion or CAF-ECM-dense regions, where diffusion and clearance are constrained (3,47).

The polyamine cloud should be viewed as a conceptual framework for evidence of organizational dispersion rather than a unified mechanism fully validated across all cancer types. Its primary value lies in providing operational standards for treatment sequences. When a stable polyamine cloud exists, directly enhancing the Output layer through ferroptosis sensitization may not be the best choice. Instead, disrupting the cloud-maintaining cycle may need to occur prior to ferroptosis induction, especially in myeloid-dominant tumors with active polyamine uptake-efflux cycling. Otherwise, treatment may induce inflammatory stress without sufficient tumor-cell killing, thereby favoring suppressive myeloid recruitment and limiting therapeutic efficacy.

The catabolic axis: SAT1-PAOX/SMOX as oxidative triggers linking polyamine state to lipid peroxidation. The core significance of polyamine catabolism lies in its ability to convert the State-layer polyamine program into directed oxidative inputs. Polyamine oxidation generates H_2O_2 and aldehyde byproducts, which can increase local oxidative pressure and push membrane lipid-peroxidation kinetics toward the ferroptosis execution threshold. Therefore, the catabolic axis is not merely about reducing polyamine abundance; it determines whether buffering polyamine status is redirected toward the amplification of oxidative stress.

Spermidine/spermine n1-acetyltransferase (SSAT)/SAT1-PAOX Axis: Acetylation-guided flux routing and peroxisomal oxidative output. In mammalian cells, the canonical polyamine catabolic pathway involves SAT1-mediated acetylation, followed by PAOX-mediated oxidative back-conversion. SAT1, also known as SSAT1, acetylates spermine and spermidine, generating N^1-acetylated polyamines that can be exported or oxidized by the peroxisomal PAOX, also known as acetylpolyamine oxidase (APAO). PAOX converts these acetylated substrates into lower-order polyamines while generating H_2O_2 and aldehyde-derived stress signals (48,49).

Functionally, SAT1 acts as a flux gate. It shifts the polyamine pool from structural binding or buffering to efflux and oxidative catabolism. PAOX serves as a peroxisomal execution module, converting these redirected substrates into oxidative products. The SAT1-PAOX axis links polyamine turnover to redox stress and establishes a mechanistic bridge between polyamine status and ferroptosis vulnerability (50).

The SMOX axis: Direct spermine oxidation, H_2O_2 production and acrolein-related carbonyl stress. In parallel with the SAT1-PAOX pathway, SMOX directly oxidizes spermine to spermidine while producing H_2O_2 and 3-aminopropanal. The latter can further convert into reactive carbonyl species, including acrolein, thereby exacerbating protein damage, membrane-lipid injury and oxidative stress (51-53). In inflammation-associated tumors, increased SMOX activity may thus convert inflammatory inputs into oxidative and carbonyl stress. This is particularly relevant in myeloid-dominated microenvironments where inflammation is present but immune execution is inefficient. Under these conditions, SMOX-mediated catabolism may elevate basal lipid-peroxidation pressure and bring the system closer to the ferroptosis threshold (41,54,55).

SAT1-arachidonate 15-lipoxygenase (ALOX15) coupling: From catabolic flux to ferroptosis execution. Among the links between polyamine catabolism and ferroptosis, the SAT1-ALOX15 axis provides one of the clearest mechanistic examples. Ou *et al* (56) demonstrated that p53 transcriptionally activates SAT1, while SAT1 induction promotes lipid peroxidation, ferroptosis and tumor-growth suppression under oxidative stress conditions. Mechanistically, SAT1 upregulation is accompanied by increased ALOX15 expression, and pharmacological inhibition of ALOX15 rescues the ferroptosis phenotype induced by SAT1. These findings suggest that SAT1 not only increases polyamine turnover; it couples catabolic flux to membrane phospholipid peroxidation through a lipoxygenase-dependent amplifier, thereby promoting lethal lipid-peroxidation accumulation and ferroptosis execution.

Polyamine catabolism-ferroptosis amplification in cancer therapy. Beyond the canonical p53-SAT1-ALOX15 pathway, recent studies further support the notion that polyamine metabolism can amplify the vulnerability to ferroptosis in cancer therapy. A 2024 study proposed polyamine-mediated ferroptosis amplification as a targetable vulnerability, indicating that polyamine metabolism can expose therapeutically relevant susceptibility to ferroptosis (3). A more recent 2025 study linked this principle to KRAS-targeted therapy, showing that polyamines sensitize KRAS-mutant tumors to KRAS inhibition, and this sensitivity depends on the status of kelch-like ECH-associated protein 1 (KEAP1), with SAT1-mediated polyamine catabolism being essential for this ferroptosis-related response (57).

These findings collectively establish a universal mechanistic principle: Polyamine catabolism is not merely correlated with ferroptosis but dictates whether therapeutic interventions induce lethal lipid-peroxidation stress. The executability of this axis depends on whether SAT1-mediated flux routing is involved and whether downstream oxidative outputs, including PAOX- or SMOX-associated pathways, are sufficient to push the system beyond the ferroptosis threshold. Therefore, the polyamine catabolism-ferroptosis axis provides a state-dependent vulnerability that can be exploited in rational combination therapies.

Summary: Catabolic flux maps polyamine state onto the ferroptosis threshold. Overall, the polyamine catabolic axis contains two major oxidative-output pathways: The SAT1-guided acetylation/back-conversion pathway through PAOX and the SMOX-mediated direct oxidation of spermine. Although these two pathways differ in substrate preference, subcellular localization and byproduct characteristics, both generate H_2O_2 and aldehyde-induced carbonyl stress, thereby elevating lipid-peroxidation pressure.

Importantly, polyamine catabolism should not be viewed merely as a terminal clearance step of polyamine metabolism. In the p53-SAT1-ALOX15 model, catabolic flux can couple with membrane phospholipid peroxidation through amplifiers dependent on lipoxygenases, thereby making the turnover of polyamines to ferroptosis execution more efficient. Thus, the catabolic axis serves as a critical interface that converts the State layer into the Output layer. The strength and direction of this mapping depend on SAT1-mediated flux routing, PAOX- or SMOX-associated oxidative outputs, subcellular localization and the availability of lipid-peroxidation amplifiers such as ALOX15.

Polyamines and immunosuppression: Myeloid polarization and T-cell functional recovery. Polyamines are not merely growth-associated metabolites of tumor cells; they also act as immunoregulatory state variables in the TME. Changes in the synthesis, uptake, efflux and catabolism of polyamines can reshape myeloid polarization, impair antigen presentation and limit T-cell effector differentiation. In this manner, polyamine flux locks the T-cell functional impairment induced by Input-layer arginine depletion into a sustained immunosuppressive state, helping explain why T cells struggle to recover once local arginine availability drops below a functional threshold (58,59).

This suppressive effect can be understood through three interconnected mechanisms. First, polyamine homeostasis is coupled with an inhibitory myeloid phenotype. ARG-driven myeloid cells consume arginine and generate ornithine, thereby supporting polyamine biosynthesis; in turn, a polyamine-rich environment may help maintain or polarize myeloid cells into an immunosuppressive state, including M2-like TAMs and MDSCs (42). Second, polyamines may weaken the initiation of adaptive immunity by impairing dendritic-cell maturation and antigen-presenting capacity, thereby reducing sustained antigenic stimulation and costimulatory support for T cells (59).

Third, extracellular polyamines can directly limit the metabolic plasticity of T cells. In pancreatic ductal adenocarcinoma, tumor-derived spermine reduced cytosolic and mitochondrial Ca^{2+} availability in $CD8^+$ T cells and inhibited the phosphorylation of mechanistic target of rapamycin, ribosomal protein S6 kinase (S6K) and eukaryotic translation initiation factor 4E-binding protein 1. These changes were accompanied by reductions in glycolysis, tricarboxylic acid cycle activity and oxidative phosphorylation, impaired mitochondrial fitness, decreased adenosine triphosphate production and reduced T-cell proliferation and cytotoxic-effector production. Spermine exposure also decreased the expression of granzyme B, IFN-γ, tumor necrosis factor-α and perforin, providing a direct mechanistic link between a spermine-rich TME, mechanistic target of rapamycin complex 1 (mTORC1) inhibition and $CD8^+$ T-cell dysfunction (60). Experimental disruption of tumor spermidine production restored $CD8^+$ T-cell activity and improved the efficacy of immune-checkpoint blockade in pancreatic cancer models.

Polyamine-dependent T-cell state regulation also extends to epigenetic programming. In $CD4^+$ T cells, disruption

of ODC1-dependent polyamine synthesis altered histone acetylation and led to a loss of fidelity in helper-T-cell lineage. Spermidine also provides the aminobutyl substrate required for eukaryotic translation initiation factor 5A (eIF5A) hypusination, linking polyamine availability to mitochondrial metabolism, protein translation and the maintenance of appropriate transcriptional programs (43). Thus, polyamine flux can influence not only short-term nutrient sensing but also the chromatin and transcriptional states that determine T-cell differentiation and functional plasticity.

Importantly, existing evidence does not demonstrate that every extracellular polyamine-rich niche induces the same epigenetic program. Currently, the strongest direct causal evidence is in pancreatic cancer, where spermine-mediated mTORC1 inhibition and mitochondrial metabolism are observed, while the findings of histone acetylation and eIF5A-hypusination primarily showcase how intracellular polyamine availability regulates T-cell lineage identity. Thus, the polyamine cloud should be interpreted as a source of sustained polyamine exposure at the tissue level, which can translate into metabolic and epigenetic effects after cellular uptake, rather than as a single universally validated inhibitory pathway. These mechanisms collectively explain how Input-layer arginine depletion can be stabilized at the State layer through myeloid polarization, impaired antigen presentation, reduced T-cell metabolic fitness and altered lineage programming.

4. The ferroptosis threshold as an executable therapeutic output

Ferroptosis is not a binary present-or-absent phenotype, but rather a critical state transition determined by the balance between lipid-peroxidation pressure and anti-ferroptotic buffering capacity (44). In the present review, the ferroptosis threshold referred to the minimum net perturbation required to drive lipid peroxidation from a reversible adaptive zone into irreversible membrane damage and cell-death execution under a given cellular state and microenvironmental context.

A lower threshold indicates that endogenous stress or therapeutic interventions can more easily trigger ferroptosis, while a higher threshold allows tumor cells to tolerate oxidative pressure and maintain fitness. Therefore, therapies targeting ferroptosis should not be simplified to merely adding ferroptosis inducers. Instead, it requires defining whether the intervention strengthens the triggering arm, weakens the buffering arm or bypasses compensatory ferroptosis defenses that may mask the true vulnerability of the system. Only when the Output layer aligns with the Input and State layers, by considering oxidative baselines, substrate allocation, polyamine flux and spatial nutrient supply, can ferroptosis induction become a predictable and stratifiable therapeutic window. Fig. 4 summarizes the balance between ferroptosis triggers and buffering systems.

Trigger modules: Polyunsaturated fatty acid-containing phospholipid (PUFA-PL) loading and lipoxygenase (LOX)-mediated lipid-peroxidation amplification. The ferroptosis triggering module refers to the initiation and amplification of lipid-peroxidation chain reactions. It is determined by two interrelated requirements: The availability of peroxidizable membrane substrates, primarily PUFA-PLs, and the presence of catalytic systems that ignite and propagate oxidative damage. acyl-CoA synthetase long-chain family member 4 (ACSL4) and lysophosphatidylcholine acyltransferase 3 (LPCAT3) facilitate the integration of PUFAs into membrane phospholipids, while ALOX15, cytochrome P450 oxidoreductase (POR) and unstable iron pools provide directional oxidation, free radical initiation and Fenton-driven amplification (61,62). Therefore, the triggering module is not a single molecular switch but a dynamic process composed of substrate loading, oxidative ignition and chain propagation.

This concept provides operational standards for stratification. In tumors with abundant PUFA-PL substrates and complete amplification chains, the inhibition of the cystine/glutamate antiporter system x_c^- or an increase in ROS input is more likely to translate into executable ferroptosis. By contrast, in tumors with substrate scarcity, weak lipid-peroxidation mechanisms, or limited iron supply, merely adding a ferroptosis inducer may be insufficient to cross the execution threshold. In such contexts, ferroptosis-targeted therapy should be aligned with upstream Input- and State-layer interventions that reshape substrate loading, iron availability or oxidative baseline, thereby creating a more predictable therapeutic window.

Substrate loading: The ACSL4-LPCAT3 axis and ferroptosis-competent membranes. Ferroptosis sensitivity is strongly influenced by the composition of membrane lipids. PUFAs only become lethal substrates for lipid-peroxidation chain reactions when incorporated into membrane phospholipids, particularly PE and phosphatidylcholine (63). ACSL4 activates ω-6 PUFAs, such as arachidonic acid and adrenic acid, into acyl-CoA derivatives and promotes their incorporation into phospholipid species. Genetic and multi-omics evidence suggests that ACSL4 is a key determinant of ferroptosis susceptibility, and the loss of ACSL4 reduces PUFA-phospholipid loading and oxidized lipid death signals, thereby conferring ferroptosis resistance (45,63,64).

LPCAT3 further esterifies activated PUFA-CoA into membrane phospholipids, generating a pool of peroxidizable substrates rich in PUFAs, located on organelle membranes and the plasma membrane (65). Together, ACSL4 and LPCAT3 act as a substrate-programming module that determines whether the membrane is ferroptosis-competent. High levels of ACSL4-LPCAT3 activity increase the density of peroxidizable sites and reduce the perturbation required to execute ferroptosis, while weak substrate loading raises the execution threshold. This may help explain why tumors, or even distinct microdomains within a single tumor, exhibit variable sensitivities to ferroptosis inducers despite comparable basal antioxidant defenses (66).

Directional oxidation: The phosphatidylethanolamine-binding protein 1 (PEBP1)-ALOX15 axis directs peroxidation toward PE. Ferroptosis is not equivalent to random lipid oxidation. In multiple models, lipoxygenase-mediated oxidation generates specific oxidized PUFA-containing PE species, which serve as executable ferroptotic signals. Wenzel *et al* (62) demonstrated that PEBP1 can form a complex with 15-LOX and alter its substrate preference toward PE, thereby promoting pro-ferroptotic PE oxidation. This mechanism transforms lipid peroxidation from nonspecific oxidative noise into a more directional execution program.

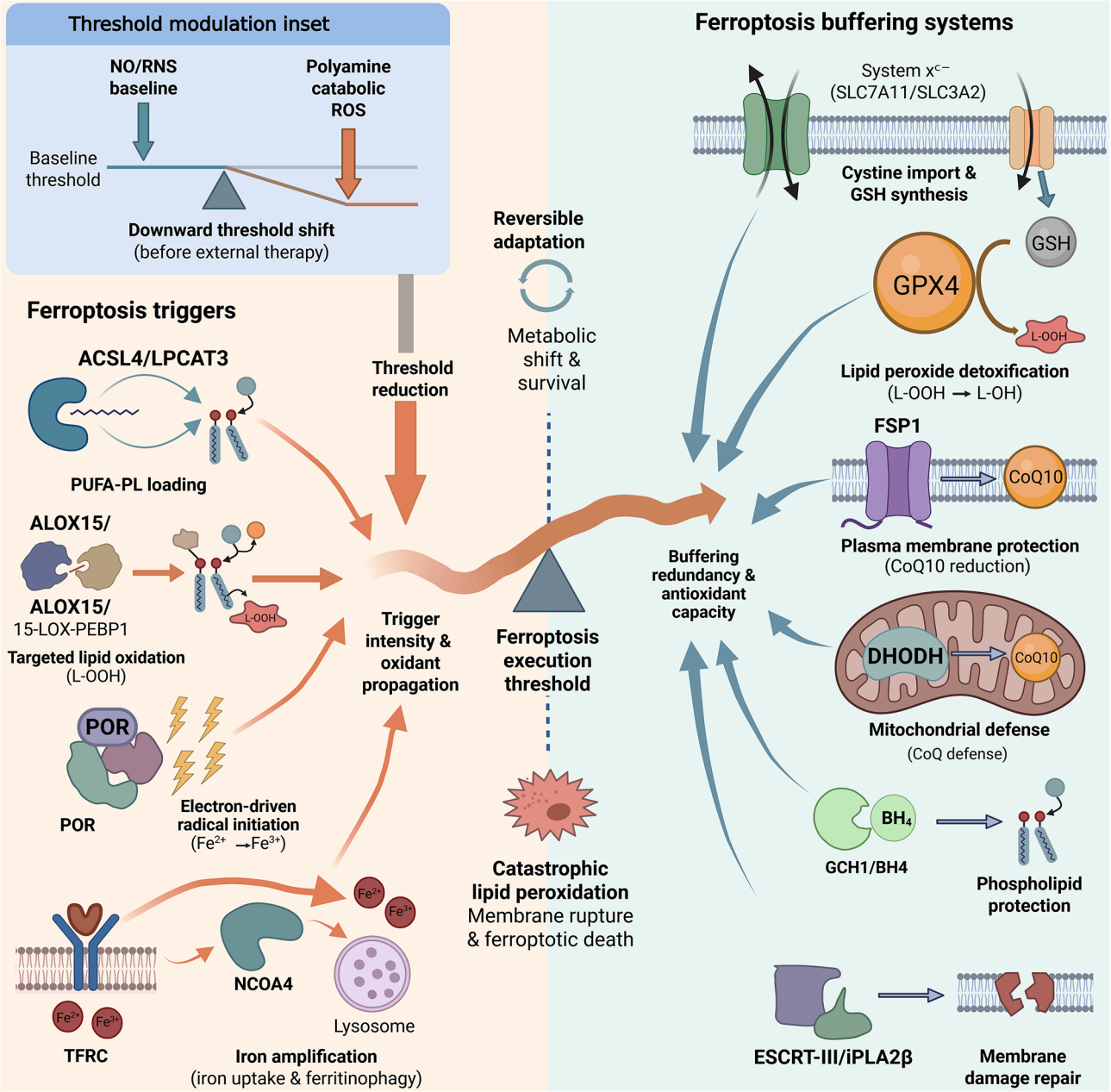

Figure 4. Ferroptosis threshold defined by trigger modules and buffering systems. ACSL4/LPCAT3, ALOX15/PEBP1, POR and iron-loading modules promote lipid-peroxidation propagation, whereas the system x_c^--GSH-GPX4 axis, FSP1-CoQ10, DHODH, GCH1/BH4 and membrane-repair systems provide redundant buffering. ACSL4, acyl-CoA synthetase long-chain family member 4; LPCAT3, lysophosphatidylcholine acyltransferase 3; ALOX15, arachidonate 15-lipoxygenase; 15-LOX, 15-lipoxygenase; PEBP1, phosphatidylethanolamine-binding protein 1; POR, cytochrome P450 oxidoreductase; NO/RNS, nitric oxide/reactive nitrogen species; ROS, reactive oxygen species; PUFA-PL, polyunsaturated fatty acid-containing phospholipids; TFRC, transferrin receptor; NCOA4, nuclear receptor coactivator 4; system x_c^-, cystine/glutamate antiporter; SLC7A11, solute carrier family 7 member 11; SLC3A2, solute carrier family 3 member 2; GSH, glutathione; GPX4, glutathione peroxidase 4; FSP1, ferroptosis suppressor protein 1; CoQ10, coenzyme Q10; DHODH, dihydroorotate dehydrogenase; GCH1, GTP cyclohydrolase 1; BH_4, tetrahydrobiopterin; ESCRT-III, endosomal sorting complex required for transport III; iPLA2β, calcium-independent phospholipase A2 β; L-OOH, lipid hydroperoxide; L-OH, lipid alcohol.

This directional oxidation also connects the Output layer with the aforementioned polyamine catabolic axis. The SAT1-mediated catabolic routing can increase oxidative pressure through polyamine turnover and is associated with ALOX15-dependent lipid-peroxidation amplification (56). Therefore, ALOX15/PEBP1 should not only be interpreted as a marker of oxidative stress but also as an indicator of directional ferroptosis execution capacity. For therapeutic stratification, ALOX15/PEBP1 can be interpreted alongside SAT1, PAOX and SMOX to identify tumors where catabolic flux and lipid-peroxidation mechanisms are consistent, thereby making it more likely for the system to cross the ferroptosis threshold.

Non-enzymatic propagation: POR-mediated radical priming and chain reaction amplification. In addition to LOX-dependent oxidation, ferroptotic lipid peroxidation can also propagate through non-enzymatic free-radical processes. Using a clustered regularly interspaced short palindromic repeats (CRISPR) inhibition screening, Zou *et al* (67) identified NADPH-POR as a common requirement for ferroptosis

across multiple cell lineages. POR can transfer electrons from NADPH to oxygen-dependent redox reactions, generating radical-priming signals that promote PUFA-phospholipid peroxidation.

Functionally, POR enhances the 'spark intensity' of the triggering module. Its effect depends on the redox baseline established by the Input and State layers. In tumor states characterized by elevated NO/RNS, mitochondrial ROS leakage or oxidative inputs derived from polyamine metabolism, POR-mediated radical priming may more readily initiate lipid-peroxidation chain reactions and reduce the additional perturbation required to execute ferroptosis. For stratification, POR and related NADPH-dependent redox flux indicators may help distinguish tumors with strong oxidative ignition capabilities from those primarily driven by downstream buffering systems that confer ferroptosis resistance.

Iron supply and amplification: Transferrin receptor 1 (TFRC)-mediated uptake and nuclear receptor coactivator 4 (NCOA4)-dependent ferritinophagy. Labile iron availability promotes lipid-radical chain reactions through Fenton chemistry and supports iron-dependent enzymes involved in directed phospholipid peroxidation, including members of the lipoxygenase family (68). The size of the labile iron pool is determined by the coordinated balance among iron uptake, intracellular storage and release and cellular export. TFRC-mediated endocytosis increases the import of transferrin-bound iron, while NCOA4-dependent ferritinophagy releases ferritin-sequestered iron into the exchangeable intracellular pool. Ferroportin 1 (FPN1), encoded by solute carrier family 40 member 1 (SLC40A1), balances these processes by exporting intracellular iron and is currently considered the primary cellular iron-efflux transporter. Therefore, increased TFRC activity, enhanced NCOA4-dependent ferritin degradation or reduced FPN1 abundance can increase the labile Fe^{2+} pool and promote susceptibility to ferroptosis, while retention or increased efflux mediated by FPN1 reduces the availability of intracellular iron and may confer ferroptosis resistance.

FPN1 expression and functional activity are tightly regulated at both transcriptional and post-translational levels. Hepcidin binds to FPN1 and promotes its internalization and degradation, thereby limiting iron export and increasing intracellular iron retention. In tumor models, additional regulatory programs can modify FPN1 expression or stability. For example, sterol O-acyltransferase 1-dependent maintenance of SLC40A1 expression increased iron efflux and reduced glioma sensitivity to ferroptosis, while loss of anterior gradient 2 activated a p53-dependent program that reduced FPN1 expression, leading to intracellular iron accumulation and making pancreatic cancer cells sensitive to ferroptosis. Post-translational ubiquitination of SLC40A1 has also been shown to reduce FPN1 protein stability and increase ferroptosis sensitivity in glioma stem-like cells. These findings suggest that FPN1 is not merely a passive iron-export marker but a dynamically regulated ferroptosis checkpoint located downstream of oncogenic, stress-response and protein-degradation pathways.

At the Output layer, the combination of increased iron uptake, enhanced ferritin iron release and impaired iron export strengthens the executability of ferroptosis by combining Fenton-driven free radical amplification with iron-dependent lipid oxidation. However, the biological consequences depend on the cell type. In tumor cells, loss of FPN1 may create a therapeutic vulnerability to ferroptosis, whereas in tumor-infiltrating immune cells, excessive iron retention may instead promote ferroptosis and impair antitumor function (68). Recent experimental evidence suggests that tumor-derived hepcidin and chronic T-cell receptor stimulation reduce SLC40A1 in $CD8^+$ tumor-infiltrating lymphocytes, leading to intracellular iron accumulation, lipid peroxidation, ferroptosis and functional exhaustion, while restoration of SLC40A1 protects these cells and maintains cytotoxic activity (69).

The susceptibility to ferroptosis may thus become spatially heterogeneous, with iron-rich and oxidative-stress-high microdomains being more readily pushed across the execution threshold. For stratification, TFRC and NCOA4 should be assessed alongside FPN1/SLC40A1 and related hepcidin-related markers, rather than interpreted independently. These iron-handling markers can further be integrated with NOS2, ARG1/ARG2 and SAT1/SMOX to identify regions where iron influx, ferritin iron release and restricted export converge, thereby creating an executable ferroptosis window. Additionally, cell-type-resolved assessment is required to distinguish a desirable tumor-cell ferroptosis vulnerability from potentially harmful ferroptosis of $CD8^+$ T cells or other antitumor immune populations (68,69).

Buffering modules: GPX4 and parallel anti-ferroptotic defenses. If the trigger module determines whether lipid peroxidation can be initiated, the buffering module determines whether this damage can be neutralized before ferroptosis execution. Ferroptosis defense is not governed solely by the system x_c^--GSH-GPX4 axis, but is organized as a redundant, compartmentalized network that includes FSP1-DHODH-coenzyme Q (CoQ)10 on the plasma membrane, CoQ on the mitochondrial inner membrane, pathways for oxidized phospholipid repair or clearance and membrane-repair mechanisms (68).

These buffering systems collectively define the effective ferroptosis threshold. Robust buffering capacity allows tumor cells to withstand high oxidative pressure without undergoing ferroptosis, while impaired or bypassed buffering makes lipid-peroxidation stress more likely to become executable (70). Therefore, stratifying ferroptosis sensitivity requires assessing not only the trigger intensity but also the availability of parallel ferroptosis defenses that may mask therapeutic vulnerabilities.

The core axis: System x_c^--GSH-GPX4 axis as a common threshold pivot. The system x_c^-, composed of SLC7A11 and solute carrier family 3 member 2 (SLC3A2), imports cystine and thereby supports GSH synthesis. GPX4 then utilizes GSH to reduce phospholipid hydroperoxides, preventing the propagation of lipid-peroxidation chains and serving as a central pivot for the ferroptosis threshold (70).

However, GPX4 is not a tumor-specific vulnerability. Inducible Gpx4 deletion in adult mice leads to acute renal failure and early death, indicating that renal tissue largely relies on GPX4-mediated control of lipid peroxidation and defining the major safety boundary for systemic, non-selective GPX4 inhibition (71). This evidence comes from genetic mouse models and should not be presented as clinical adverse events for GPX4 inhibitors. Direct GPX4 inhibitors remain

largely in the preclinical research stage and their tolerability, dose-limiting toxicities and therapeutic windows in patients have yet to be determined.

Therefore, risk mitigation strategies focus on reducing the intensity and duration of GPX4 inhibition while limiting its distribution in normal tissues. Rather than starting with sustained maximal systemic GPX4 blockade, a state-matched sequence could first lower the tumor ferroptosis threshold through immune-derived IFN-γ signaling, system x_c^--GSH disruption or inhibition of a dominant bypass pathway such as FSP1 or DHODH. Short-term, intermittent or windowed GPX4 inhibition should only be introduced when pharmacodynamic evidence indicates that the tumor has entered a ferroptosis-sensitive state. This sequence may reduce the exposure required for tumor-cell killing, although its safety advantages still need prospective validation.

Tumor-selective delivery provides an additional mitigation strategy. Tumor microenvironment-activated conjugates, prodrugs, nanoparticles and cell-type-selective degraders may restrict GPX4 inhibition to malignant tissues and reduce exposure in kidneys and other normal organs that depend on GPX4 (72). As an instance, a preclinical tumor-microenvironment-activated peptide-ferriporphyrin conjugate, for example, improved tumor accumulation and locally enhanced GPX4 inhibition in multiple tumor models (72). Clinical translation also requires gradual dose escalation, baseline and during-treatment renal function assessments and treatment interruption upon evidence of renal injury or excessive systemic lipid peroxidation. These approaches should be viewed as recommended safety principles rather than clinically validated dosing standards.

Parallel defense I: FSP1-CoQ10 and vitamin K-linked GPX4-independent protection. FSP1, also known as apoptosis-inducing factor mitochondria-associated 2, has been identified as a potent GPX4-independent ferroptosis inhibitor. It reduces CoQ10 to ubiquinol using NAD(P)H, which is a lipophilic radical-trapping antioxidant that can prevent lipid-peroxidation propagation across the plasma membrane (73,74). A study has further associated FSP1-dependent reductive activity with vitamin K-mediated ferroptosis resistance, expanding the scope of GPX4-independent buffering (75).

This finding has direct implications for state-matched therapies. The standalone GPX4 or system x_c^- status may be insufficient to predict ferroptosis sensitivity, as FSP1-CoQ10 or related reductive bypass defenses can prevent lipid-peroxidation stress from becoming executable. If these bypass systems are not assessed, interventions targeting the system x_c^--GSH-GPX4 axis may produce molecular perturbation without cell-death execution. Therefore, FSP1 should be included in the minimal ferroptosis-threshold panel to identify tumor states that require the removal of bypasses to achieve effective ferroptosis output.

Parallel defense II: DHODH-CoQ provides mitochondrial ferroptosis buffering. DHODH provides compartment-specific ferroptosis defense at the mitochondrial inner membrane. Mao *et al* (76) showed that DHODH promotes CoQ reduction and cooperates with mitochondrial GPX4 to inhibit ferroptosis. Pharmacological inhibition of DHODH by brequinar selectively induces ferroptosis in GPX4-low tumors, while in GPX4-high environments, DHODH inhibition synergizes with system x_c^- inhibition, such as sulfasalazine.

From a state-stratification perspective, DHODH reveals that ferroptosis buffering is compartmentalized. If FSP1-mediated protection is weak, tumor cells may appear vulnerable at the plasma membrane, but are still protected through DHODH-dependent CoQ reduction in the mitochondrial compartment. This hidden mitochondrial buffering may explain the specific differences in tissue or model responses to ferroptosis-inducing strategies. Therefore, Output-layer stratification should assess DHODH along with GPX4 and FSP1 to distinguish insufficient triggering intensity from strong compartment-specific bypass protection.

Parallel defense III: GCH1-BH4 provides substrate-level antioxidant protection. The GCH1-BH4 axis represents another GPX4-independent buffering mechanism. Kraft *et al* (77) showed that GCH1-driven BH4 production protects cells from ferroptosis by acting as a potent antioxidant system and reshaping phospholipid composition, particularly by protecting highly peroxidizable PUFA-containing phospholipids. Through this substrate-level antioxidant protection and lipid remodeling, the GCH1-BH4 axis enhances the buffering capacity against ferroptosis and makes lipid-peroxidation stress less likely to become executable.

This mechanism has direct implications for therapeutic design. Sensitivity to ferroptosis can be altered not only by targeting GPX4 or parallel reductive systems but also by modifying the oxidizability of membrane substrates. In tumors, high GCH1-BH4 activity may indicate substrate-protective buffering and reduced ferroptosis sensitivity, suggesting that sensitization at the substrate level is needed, rather than just targeting the GPX4 axis. Conversely, in cases where it is desirable to protect normal tissues from ferroptosis damage, enhancing this axis may be beneficial. Therefore, for Output-layer stratification, GCH1/BH4-related markers may complement GPX4, FSP1 and DHODH to define effective ferroptosis thresholds.

Terminal defense: Membrane repair and peroxidized-lipid clearance. The physical endpoint of ferroptosis is the loss of membrane integrity. The endosomal sorting complex required for transport III (ESCRT-III) is a membrane-remodeling mechanism involved in repairing damaged plasma membranes, which can delay ferroptosis during lipid-peroxidation stress. Nanopores and Ca^{2+} influx associated with ferroptosis further activate ESCRT-III repair, thereby modulating death kinetics and potentially affecting the immunological consequences of ferroptotic tumor-cell death (78,79).

Meanwhile, calcium-independent phospholipase A2 beta (iPLA2β), encoded by PLA2G6, is an enzyme that hydrolyzes and detoxifies peroxidized phospholipids, including oxidized PE species such as 15-hydroperoxyeicosatetraenoyl-phosphatidylethanolamine. This mechanism provides an additional layer of protection under GPX4-deficient or p53-driven ferroptosis pressure, indicating that terminal membrane repair and peroxidized-lipid clearance can buffer the final execution phase of ferroptosis (80,81).

Overall, the buffering module consists of a segregated and compensatory defense network, including the canonical system x_c^--GSH-GPX4 axis, FSP1-CoQ10 protection at the plasma membrane, DHODH-CoQ activity at the mitochondrial inner

membrane, GCH1-BH4-mediated substrate protection and terminal damage-control mechanisms involving ESCRT-III and iPLA2β. For clinically actionable stratification, the minimal Output-layer panel should include SLC7A11/GPX4, FSP1 and DHODH, with additional assessment of GCH1-BH4 activity and markers of membrane repair or peroxidized-lipid clearance as appropriate. This panel may distinguish truly ferroptosis-sensitive tumors from those with parallel defenses that could lead to intrinsic or adaptive treatment resistance.

Compensatory crosstalk and therapeutic resistance. These ferroptosis-defense pathways do not operate independently. Instead, they provide partially redundant protection across different subcellular compartments and stages of ferroptosis execution. The system x_c^--GSH-GPX4 axis directly removes phospholipid hydroperoxides, while FSP1-CoQ10 and DHODH-CoQ maintain radical-trapping ubiquinol pools at the plasma membrane and mitochondrial inner membrane, respectively. GCH1-derived BH4 reduces membrane oxidation by trapping radicals and remodeling phospholipids, while iPLA2β and ESCRT-III further act downstream by removing oxidized phospholipids or repairing damaged membranes (73,74,76-81). Therefore, disrupting one arm of defense may increase functional dependence on another without necessarily causing uniform transcriptional upregulation.

GPX4 inhibition provides the clearest example of this compensatory organization. High FSP1 activity can maintain plasma-membrane protection and confer resistance to GPX4 inhibition through GPX4-independent CoQ10 reduction (73,74). In KEAP1-inactivated mutant lung cancer, nuclear factor erythroid 2-related factor 2-dependent transcriptional activation of FSP1 further enhances this bypass pathway and promotes resistance to ferroptosis-inducing therapies (82). However, this adaptive increase in FSP1 is genotype-dependent and should not be interpreted as a universal response to GPX4 inhibition.

DHODH provides a related but compartment-specific form of compensation. DHODH-mediated CoQ reduction cooperates with mitochondrial GPX4 to inhibit mitochondrial lipid peroxidation. Experimental DHODH inactivation preferentially induces ferroptosis in GPX4 low-expressing cancer cells, while in the case of high GPX4 expression, DHODH inhibition combined with system x_c^- blockade is necessary (76). Therefore, DHODH-mediated resistance is more accurately described as an increased functional dependence on mitochondrial CoQ reduction rather than a consistent compensatory upregulation of DHODH expression.

Compensation may also occur at the substrate and terminal-damage levels. The reduced activity of GCH1-BH4 decreases the abundance and oxidation of phospholipids sensitive to ferroptosis, thereby reducing the oxidative burden on GPX4, FSP1 and DHODH (77). Even after lipid peroxidation has been initiated, iPLA2β-mediated phospholipid clearance and ESCRT-III-mediated membrane repair can delay or prevent irreversible membrane failure (78-81). These layered defensive mechanisms explain why SLC7A11 or GPX4 inhibition can induce detectable oxidative stress at the biochemical level without complete ferroptosis execution.

This compensatory network has a direct effect on treatment resistance. Therefore, the expression of GPX4 or SLC7A11 alone may be insufficient to predict sensitivity to ferroptosis. Tumors with high FSP1 activity, strong mitochondrial DHODH dependence, active GCH1-BH4 metabolism, or effective terminal membrane-damage control may still maintain resistance despite disrupting the canonical GPX4 pathway. Therefore, rational combination therapies should target the major compensatory defenses identified in each tumor state, rather than indiscriminately suppressing all ferroptosis-protective pathways.

State interface: NO/RNS and polyamine catabolism reprogram the ferroptosis threshold baseline. The Output-layer ferroptosis threshold is not determined in isolation. It depends on the redox baseline and substrate-allocation state established by the Input and State layers. Two upstream modulators are particularly important: NOS-mediated NO/RNS production, which converts arginine into nitrosamines and oxidative stress, and polyamine catabolism, which generates oxidative inputs related to H_2O_2 and aldehydes through the SAT1-PAOX/SMOX-related pathways.

This leads to a layered operational principle: The ferroptosis threshold is not a single-variable function of ferroptosis-pathway expression, but a joint function of the oxidative baseline, substrate loading and buffering redundancy. Therefore, Output-layer assessments should integrate upstream Input/State markers with downstream triggering and buffering modules. NOS2, ARG1/ARG2 and SAT1/SMOX can serve as explanatory variables for threshold shifts, while ACSL4/LPCAT3 and TFRC/NCOA4 define substrate- and iron-dependent triggering capabilities. In parallel, SLC7A11/GPX4, FSP1 and DHODH indicate the strength of ferroptosis buffering. This coupled layered framework provides a basis for therapeutic sequences: the Input and State layers should be calibrated first, either by reducing inhibitory baseline stress or by disrupting state-locking circuits, before applying the Output-layer ferroptosis amplification. Only through this alignment can molecular perturbation more reliably translate into tumor-cell death and effective immune feedback.

Direct molecular cross-talk and context-dependent effects. The relationship among arginine metabolism, polyamine homeostasis and ferroptosis is supported by several direct regulatory axes, not merely metabolic coexistence. ARG1/ARG2 converts arginine into ornithine, which subsequently participates in polyamine synthesis via ODC1. The polyamine catabolism associated with SAT1, PAOX and SMOX can generate H_2O_2 and aldehyde-related oxidative stress, thereby increasing lipid-peroxidation pressure. In addition, iron overload has been shown to activate WNT/MYC-dependent ODC1 transcription, establishing an iron-WNT/MYC-ODC1-polyamine-H_2O_2 positive-feedback loop that amplifies ferroptosis in specific experimental models (3).

Transcriptional and epigenetic regulation further links the availability of arginine to ferroptosis and immune-cell function. The p53-SAT1 axis connects stress-responsive transcription with polyamine catabolism and ALOX15-related lipid peroxidation (56). Under arginine starvation, specific cancer cells can induce ASS1 through ATF4 and CCAAT/enhancer-binding protein beta (C/EBPβ) and utilize citrulline to restore arginine synthesis. Activated T cells, however, show reduced chromatin accessibility and increased repressive histone

modifications under arginine starvation, limiting the same adaptive response (20). Low arginine can also activate the ATF4-SLC7A11-GSH program in activated $CD4^+$ T cells and promote Treg-like immunosuppressive properties (2).

Importantly, these regulatory effects are not uniform and unidirectional. While SAT1 induction is associated with ALOX15-dependent lipid peroxidation and ferroptosis, there are also reports that SAT1 activation increases glutamine utilization and GSH synthesis in lung cancer cells, thereby supporting antioxidant adaptation and tumor-cell survival (83). Similarly, arginine deprivation may create therapeutic vulnerability in ASS1-deficient tumor cells while impairing the proliferation and cytokine production of effector T cells. The output of ferroptotic tumor cells may promote antitumor immunity in certain experimental systems, but in others, it may impair dendritic-cell maturation and antigen cross-presentation (4,84).

These apparently different observations suggest that the arginine-polyamine-ferroptosis network should be interpreted as a set of conditionally regulatory axes rather than as a single linear cascade. Biological outcomes depend on cell identity, tumor genotype, nutrient availability, polyamine routing, iron status, antioxidant capacity, drug concentration, exposure duration and the stage of ferroptosis. Accordingly, the expression of individual markers such as ARG1, ODC1, SAT1 or GPX4 cannot independently establish metabolic flux or predict treatment response. Mechanistic interpretations require cell-type-resolved measurements and, where feasible, metabolite, flux and functional validation.

5. Immune feedback determines the consequences of ferroptotic tumor-cell output

The immune system can either mediate therapeutic benefits or trigger adverse feedback responses in ferroptosis-targeted cancer therapies. Ferroptotic tumor-cell output, including oxidized lipids, damage-associated molecular patterns (DAMPs) and metabolic debris, may elicit different immune consequences depending on timing, spatial context and pre-existing immune status. In one direction, it may promote immune amplification through dendritic-cell maturation, improved cross-presentation and T-cell expansion. In the opposite direction, it may drive myeloid-mediated immunosuppressive remodeling, characterized by impaired dendritic-cell function, suppressive inflammation and the expansion of myeloid-derived suppressive populations.

Thus, the core question of the Feedback layer is not merely whether ferroptosis is immunogenic, but rather which feedback basin the Output layer may enter under a given state-map configuration. Fig. 5 illustrates how ferroptotic tumor-cell output may be converted into productive immune amplification or suppressive myeloid remodeling.

Positive feedback: IFN-gamma links t-cell effector activity to the ferroptosis threshold. The clearest template for positive immune feedback is the loop of ICB-induced $CD8^+$ T-cell activation, IFN-γ production, system x_c^- suppression, reduced antioxidant capacity and enhanced ferroptosis. Wang *et al* (85) showed that IFN-γ released by $CD8^+$ T cells downregulates SLC7A11 and SLC3A2 in tumor cells, thereby reducing cystine uptake, weakening GSH-dependent antioxidant defenses and promoting lipid peroxidation and ferroptosis. Consistently, cyst(e)ine depletion by cyst(e)inase can synergize with ICB to enhance antitumor immunity and ferroptotic tumor-cell death (85,86).

This feedback loop provides a strategic sequence for state-matching therapies. When T-cell execution remains viable, the immune response itself can act as an Output-layer threshold regulator. Sustained IFN-γ signaling weakens the system x_c^--GSH-GPX4 axis, reducing the additional perturbations required to execute ferroptosis. This explains why restoring T-cell activity prior to strong ferroptosis amplification may be more effective than directly forcing ferroptosis in immune-inflamed tumors or tumors that can be converted into a 'hot' immune state. Such restoration may require improving arginine availability, dismantling suppressive polyamines or myeloid constraints, or alleviating spatial exclusion before applying Output-layer amplification (87,88).

Negative feedback: Ferroptotic products may impair dendritic-cell processing and cross-presentation. Although ferroptosis can promote antitumor immunity, increasing evidence indicates that ferroptotic tumor-cell products may also impair antigen presentation under specific timing and compositional contexts. Wiernicki *et al* (4) showed that ferroptotic tumor cells can inhibit dendritic-cell maturation, hinder cross-presentation, and fail to induce effective tumor protection when used for dendritic-cell loading (5). These findings indicate that ferroptosis is not synonymous with immunogenic cell death; its immune consequences depend on the generation, processing, and presentation of ferroptotic materials.

In immune rejection or immune-desert tumors, negative feedback is more likely to occur, especially in environments dominated by myeloid cells. In these environments, dendritic cells and T cells are spatially separated or functionally restricted and excessive oxidized lipids or membrane-peroxidation products may exceed the antigen-processing capacity and promote suppressive inflammatory remodeling (29,89). The execution kinetics of ferroptosis may further influence this output. ESCRT-III-mediated membrane repair can delay ferroptosis and regulate membrane-pore formation, Ca^{2+} signaling and immune visibility, thereby altering the immune system's perception of dying tumor cells (78,79). Therefore, negative feedback does not imply that ferroptosis is universally detrimental; rather, it reflects a mismatch between ferroptosis output and the immune system's processing capacity.

What determines whether death output enters positive or negative feedback? Within a state-matched immunopharmacological framework, ferroptosis should not be assumed to be automatically immunogenic. The same ferroptosis output may enter opposing feedback states depending on whether it can be processed by the immune system, coupled with the effects circuit at the tissue level and whether it is released from the dominant suppressive network. Based on current evidence, the present study proposed an evidence-based but hypothesis-generating feedback-gating framework organized around three conditions that may favor positive feedback: Sufficient immune-processing capacity, spatial accessibility and lack of dominant myeloid- or polyamine-mediated suppression.

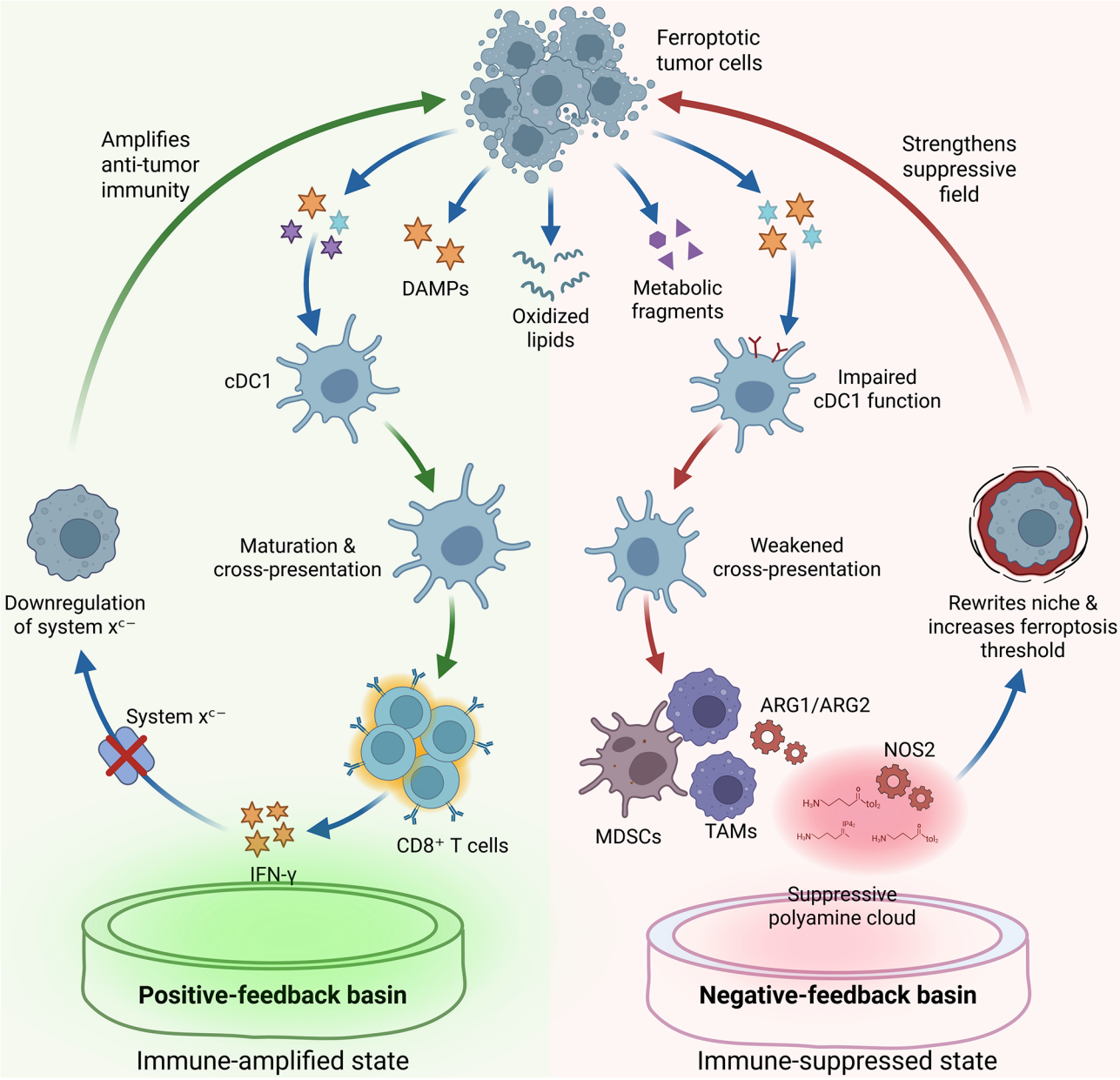

Figure 5. Immune feedback routes after ferroptotic tumor-cell output. Processable ferroptotic signals may support dendritic-cell activation, IFN-γ production and positive feedback, whereas excessive or spatially disconnected output may impair antigen presentation and promote suppressive myeloid rewriting. DAMPs, damage-associated molecular patterns; cDC1, conventional type 1 dendritic cell; CD8, cluster of differentiation 8; IFN-γ, interferon-γ; system x_c^-, cystine/glutamate antiporter; ARG1, arginase 1; ARG2, arginase 2; MDSCs, myeloid-derived suppressor cells; TAMs, tumor-associated macrophages; NOS2, nitric oxide synthase 2.

Each condition has different experimental or human-tumor evidence supporting it, as described below. However, their simultaneous requirements have yet to be prospectively validated in a single tumor cohort, and thus should be interpreted as testable gating variables rather than universally established necessary and sufficient criteria. The failure of any one condition may prevent the conversion of ferroptosis output into immune amplification. Conversely, the system may enter processing failure, suppressive myeloid remodeling and stable therapeutic tolerance. These gating conditions should not be viewed as strict categories but as an operational framework for predicting feedback direction. Their value lies in helping determine whether a given tumor state is ready for Output-layer amplification, or whether treatment should first shift upstream toward Input-layer correction, State-layer disruption or spatial preconditioning.

Is immune-processing capacity sufficient: Processable output or processing failure? The premise of positive feedback is that the output of ferroptotic tumor cells can be captured and processed by dendritic cells, promoting their maturation and supporting antigen cross-presentation, thereby translating into sustained T-cell expansion and IFN-γ-driven amplification. Experimental evidence suggests that this process largely depends on the stage and method of ferroptosis induction. In murine MCA205 fibrosarcoma and GL261 glioma models, early RSL3-induced ferroptotic cells were effectively engulfed by bone-marrow-derived dendritic cells, promoting dendritic-cell maturation and generating protective immunity

in preventive vaccination experiments, while late ferroptotic cells failed to produce comparable protection (84).

However, ferroptosis does not uniformly produce processable immune output. Using inducible GPX4 inhibition and pharmacological ferroptosis models, Wiernicki *et al* (4) reported that ferroptotic cancer cells impaired dendritic-cell maturation, reduced antigen cross-presentation and failed to protect mice from subsequent MCA205 fibrosarcoma or B16-OVA melanoma growth. These seemingly disparate findings suggest that immune-processing capacity is determined not by ferroptosis alone, but by the inducers, death stage, DAMP-release kinetics, oxidized-lipid burden, antigen cargo and the functional state of receiving dendritic cells. Early, controlled and immune-processable cell death outputs facilitate immune amplification, whereas prolonged or highly oxidized output may become a processing burden and promote negative feedback.

The immune-processing capacity can thus be viewed as the first feedback-gating condition. Surrogate indicators may include the abundance of conventional type 1 dendritic cell (cDC1), such as the basic leucine zipper ATF-like transcription factor 3, X-C motif chemokine receptor 1 and C-type lectin domain family 9 member A; dendritic-cell maturation markers, including cluster of differentiation 86, C-C motif chemokine receptor 7 and interleukin 12; as well as antigen-presentation modules, including transporter associated with antigen processing 1/2, beta-2-microglobulin and major histocompatibility complex class I-related gene sets (90-92). T-cell-side indicators include clonal expansion and IFN-γ-axis activation, with representative genes being interferon gamma gene, C-X-C motif chemokine ligand 9 and C-X-C motif chemokine ligand 10, as well as the restoration of cytotoxic and proliferative programs (93,94). Output-side readings may include lipid-peroxidation burden and oxidized-lipid species, such as 4-hydroxynonenal and oxidized PE. Insufficient immune processing capacity results in robust molecular perturbations from direct ferroptosis amplification but no effective immune activation. In this case, enhancing dendritic-cell processing capacity or reducing unprocessable oxidative outputs should precede Output-layer amplification.

Is spatial accessibility present: can death output be coupled to the dendritic cell (DC)/T-cell circuit? Even if ferroptosis outputs can be processed, if they are spatially decoupled from dendritic-cell and T-cell circuits, they may not enter positive feedback. This is particularly relevant in immune-excluded or immune-desert tumors, where CAF-ECM barriers, low perfusion and diffusion bottlenecks limit antigen capture and T-cell entry. In this case, ferroptosis may occur within the inhibitory tumor core, which has poor accessibility to immune cells. The output may not drive adaptive immune amplification but instead convert to local inflammation and myeloid-recruitment signals, thereby increasing the likelihood of negative feedback (95,96).

Although direct spatial studies linking ferroptotic tumor-cell outputs to dendritic-cell-T-cell coupling remain limited, evidence from human tumor immunology supports spatial accessibility as a biologically relevant threshold. In advanced melanoma patients receiving immune checkpoint inhibitors, the spatial proximity and interaction of cDC1s with $CD8^+$ T cells positively correlated with therapeutic response (97). By contrast, analyses of metastatic urothelial cancers treated with atezolizumab showed that transforming growth factor β (TGF-β) signaling, collagen-rich stroma and the exclusion of $CD8^+$ T cells from the tumor parenchyma were associated with treatment resistance. In immune-excluded mouse models, combined TGF-β and PD-L1 blockade restored T-cell penetration into the tumor center and promoted tumor regression (98). These studies did not directly manipulate ferroptosis, but they provide human-tumor and experimental evidence, indicating that the biological effects of local death signals depend on whether antigen-presenting cells and effector T cells are spatially connected to the area where the signal is generated.

Therefore, spatial accessibility is the second feedback-gating condition. Whether the Output layer can be perceived and written back by the Feedback layer depends not only on the composition of death output but also on whether death occurs at a location connected to immune-processing and effector circuits. If spatial accessibility is lacking, therapeutic priorities should shift from direct Output-layer amplification to coupling repairs, such as improving perfusion, reducing stromal barriers or relieving immune rejection. Otherwise, the system may enter a state of structural failure, where tumor-cell death occurs, but the immune circuit remains disconnected.

Is the myeloid/polyamine suppressive network dominant: Has negative-feedback gain been preconfigured? The third gating condition is whether the TME has been dominated by the suppression network established by myeloid activity and externalized polyamine flux. When the depletion mediated by ARG1/ARG2 and the metastasis driven by NOS continue to limit the availability of arginine, and polyamine uptake-efflux cycling sustains a suppressive cloud, the output of ferroptosis may primarily be interpreted as an additional damage signal. This can promote myeloid recruitment, reinforce ARG/NOS activity, deepen nutrient-dependent immune dysfunction and drive suppressive inflammatory remodeling. In this case, Output-layer amplification may have adverse effects: Tumor-cell killing remains insufficient, whereas immune effector cells are further depressed below their functional threshold (99,100).

Direct experimental evidence from pancreatic cancer indicates that the output of ferroptosis can be converted into tumor-promoting myeloid remodeling. Oxidative stress and autophagy-dependent ferroptosis facilitate the release of oncogenic KRAS^G12D from pancreatic cancer cells into extracellular vesicles. Macrophages internalize extracellular KRAS^G12D through advanced glycosylation end-product specific receptor (AGER), subsequently polarizing towards an M2-like tumor-promoting state via signal transducer and activator of transcription 3 (STAT3)-dependent fatty-acid oxidation. Disruption of KRAS^G12D release or macrophage uptake reduces macrophage-mediated pancreatic tumor growth, while detection of KRAS^G12D in macrophages correlates with poor survival in patients with pancreatic cancer (99). This provides a representative example in which ferroptotic tumor-cell output directly enters a negative myeloid-feedback circuit.

Hepatocellular carcinoma (HCC) provides a complementary example of polyamine-mediated suppressive feedback. N1-acetylspermidine is enriched in human HCC tissues

and paired plasma samples. Inflammatory macrophages induce the expression of SAT1 in hepatoma cells, promoting SLC3A2-dependent N1-acetylspermidine efflux. Extracellular metabolites activate SRC proto-oncogene, non-receptor tyrosine kinase (SRC) signaling, inducing C-C motif chemokine ligand 1 $(CCL1)^+$ macrophage polarization and inducing C-C motif chemokine receptor 8^+ regulatory T cells, thereby hindering immune-checkpoint blockade. Targeting SAT1, SLC3A2 or CCL1 improved the antitumor effects of checkpoint therapy in experimental models (100). Although this study did not specifically initiate the circuit through ferroptosis, it provides human-tumor and mechanistic evidence that an established polyamine-efflux network can preconfigure the TME toward suppressive feedback.

Therefore, the key issue is not whether a single suppressive molecule is upregulated, but whether the myeloid/polyamine network has gained sufficient system-level gain to prioritize the conversion of death output into suppressive remodeling rather than adaptive immune amplification. Surrogate indicators may include MDSC/TAM enrichment, ARG1/ARG2 and NOS2 expression, polyamine-related modules such as ODC1/AMD1 and SAT1/SMOX, acetylated-polyamine ratios, and additional stress signals such as cyst(e)ine limitation or antioxidant-substrate competition (32,46,54,101-105). If this suppressive network is dominant, ferroptosis amplification should be positioned as a later-stage intervention. Upfront therapy should instead prioritize dismantling myeloid/polyamine suppression, restoring Input-layer nutrient availability, disrupting State-layer locking and reducing negative-feedback gain.

Summary: Three gating conditions determine the feedback basin and therapeutic sequence. Overall, the immunological consequences of ferroptosis output should be interpreted as a gated circuit rather than an automatic result. Output-layer amplification is more likely to produce effective immune feedback only when all three conditions are simultaneously met: Sufficient immune-processing capacity, spatial accessibility and absence of dominant myeloid/polyamine suppressive-network control. If any condition is missing, the treatment sequence should shift upstream toward Input-layer correction, State-layer disruption or spatial preconditioning, rather than simply increasing ferroptosis stress.

These gating conditions should be viewed as an evidence-anchored and operational hypothesis rather than a universal rule validated across all cancer types and clinical settings. Immune-processing capacity is supported by ferroptosis-cell vaccination and dendritic-cell experiments; spatial accessibility is supported by spatially resolved human tumor studies and immune-exclusion models, while the suppressive-network dominance is supported by studies on ferroptosis-driven macrophage polarization and polyamine-mediated immune remodeling mechanisms. Nevertheless, these three conditions have primarily been studied in different experimental systems and tumor types. Their combined predictive value, relative weight, and potential cancer-specific thresholds need to be prospectively validated through spatial profiling, cell-type-resolved metabolic measurements and longitudinal treatment-response cohorts. Therefore, the current framework provides a testable decision scaffold for determining when to repair upstream conditions, when to amplify ferroptosis output and when to switch therapeutic routes.

Feedback rewriting of the input and state layers: Myeloid expansion, ARG/NOS activation and polyamine-cloud restabilization. When the aforementioned gating conditions are not met, ferroptosis output may enter a negative-feedback basin. A typical niche remodeling trajectory is initiated by oxidative stress or damage-associated signals that drive myeloid cell recruitment and expansion. These myeloid cell populations can further upregulate ARG1/ARG2 and NOS2, intensifying arginine depletion and diversion within the arginine niche and pushing local arginine flux further below the threshold required for effector T-cell activity.

Meanwhile, increased ornithine supply can reinforce polyamine synthesis and uptake-efflux cycles, leading to the restabilization of the suppressive polyamine cloud. Through this circuit, short-term death-output events may be converted into long-term niche remodeling. This feedback rewriting may contribute to post-treatment immune cooling, tumor recurrence and therapeutic tolerance.

6. State-matched immunopharmacological strategies and therapeutic sequencing

Based on the Input-State-Output-Feedback framework, cancer therapy should not be designed solely by targeting isolated metabolic nodes. A more feasible strategy is to first define the state coordinates of the tumor system and then apply sequential or combinatorial interventions to reshape the vulnerability to ferroptosis and immune execution capacity. From this perspective, treatment design shifts from node-centric inhibition to state-matching threshold modulation, where the timing, order and combination of interventions are determined by the availability of arginine, polyamine flux, ferroptosis-buffering capacity and immune-feedback potential. Fig. 6 translates this framework into a state-matching therapeutic decision diagram.

Why state mapping should precede pharmacological combination. State-matching immunopharmacological therapy should not be simplified to ferroptosis induction or immune activation alone. Identical metabolic perturbations can induce opposing biological outcomes across different tumor types, spatial microdomains and treatment stages. For example, arginine restriction may impair T-cell effector function by reducing local arginine flux below the immune functional threshold, but under specific redox and buffering conditions, it may also increase susceptibility to lipid peroxidation. Similarly, ferroptosis induction may promote immune amplification in one context while leading to dendritic-cell processing failure, suppressive myeloid remodeling or ineffective molecular perturbation in another. These different outcomes should not merely be viewed as experimental inconsistencies; rather, they reflect different state coordinates that determine the direction and executability of therapeutic output.

Based on the Input-State-Output-Feedback logic, the present study proposed state mapping as a practical framework for organizing these differences. Here, 'state mapping' does not refer to a validated pan-cancer classification system, but

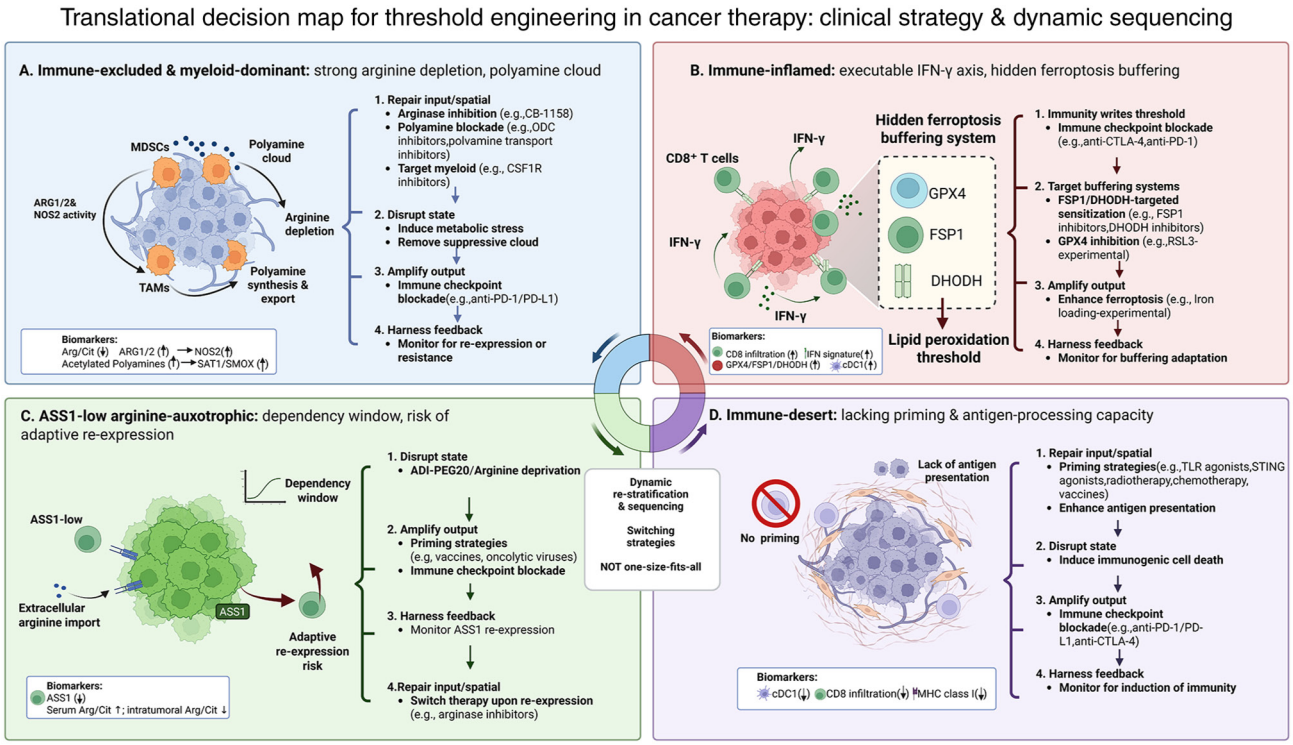

Figure 6. State-matched therapeutic decision map. Four tumor-immune prototypes are organized by dominant bottleneck, preferred therapeutic sequence, pharmacodynamic readouts and switch triggers: immune-excluded/myeloid-dominant, immune-inflamed/IFN-gamma-executable, ASS1-low/arginine-dependent and immune-desert/priming-deficient states. MDSCs, myeloid-derived suppressor cells; TAMs, tumor-associated macrophages; ARG1/2, arginase 1/arginase 2; NOS2, nitric oxide synthase 2; ODC, ornithine decarboxylase; CSF1R, colony-stimulating factor 1 receptor; Arg/Cit, arginine-to-citrulline ratio; SAT1, spermidine/spermine N1-acetyltransferase 1; SMOX, spermine oxidase; IFN-γ, interferon-γ; CD8, cluster of differentiation 8; GPX4, glutathione peroxidase 4; FSP1, ferroptosis suppressor protein 1; DHODH, dihydroorotate dehydrogenase; cDC1, conventional type 1 dendritic cell; PD-1, programmed cell death protein 1; PD-L1, programmed death-ligand 1; CTLA-4, cytotoxic T-lymphocyte-associated protein 4; ASS1, argininosuccinate synthase 1; ADI-PEG20, pegylated arginine deiminase; TLR, toll-like receptor; STING, stimulator of interferon genes; MHC class I, major histocompatibility complex class I.

rather to an operational four-dimensional coordinate model that identifies the main bottlenecks of a given tumor system: Input-layer arginine availability, State-layer polyamine flux, Output-layer ferroptosis vulnerability or Feedback-layer immune-processing capacity. The aim is to guide therapeutic sequencing; what should be corrected first, what should be amplified next, when treatment should be escalated and when a therapeutic route should be switched. Thus, state mapping is intended to organize decision logic rather than replace disease-specific biological details.

Pharmacological leverage points across the Input-State-Output-Feedback layers. Therapy can be viewed as a targeted reconfiguration of the Input-State-Output-Feedback system, rather than an isolated single-node inhibition. The stability of therapeutic efficacy depends not only on the potency of individual drugs but also on whether the intervention aligns with the current state coordinates and is delivered in a sequence that pushes the system toward an executable therapeutic window.

To enhance operational applicability, treatment strategies are organized around six decision dimensions: initial state, dominant bottleneck, priority leverage point, combination sequence, dynamic pharmacodynamic readouts and escape or state-drift trajectories, as summarized in Table II.

Four tumor-immune prototypes for therapeutic sequencing. The following four prototypes are not intended to define a strict classification system for all solid tumors. Instead, they provide a minimal translational framework for applying state matching to therapeutic sequencing. Each prototype is organized around five questions: Where the dominant bottleneck lies, which leverage point should be prioritized, how the intervention sequence should be arranged, which pharmacodynamic panel should be monitored and when the therapeutic route should be switched.

This framework does not override disease-specific biological characteristics with fixed classification categories. Instead, it provides a conceptual scaffold for comparing tumor states across different models and cancer types, translating Input-State-Output-Feedback logic into executable therapeutic rules. To operationalize these prototypes, we define candidate marker combinations and assay-based reference standards, rather than single-marker diagnostic thresholds (Table II). Prototype assignments should require concordance across at least two orthogonal evidence layers, including at least one spatial or functional measurement when feasible. 'High' and 'low' states should be prospectively defined using disease-specific reference cohorts or validated assay thresholds, rather than arbitrary post hoc median splits. Importantly, Prototypes A, B and D primarily describe immune-spatial states, whereas Prototype C describes a tumor-cell metabolic dependency. Prototype C may therefore coexist with Prototype A, B or D and should be reported as a composite state, such as C-A or C-B, when appropriate.

Table II. Prototype-based state-matching matrix for therapeutic sequencing, pharmacodynamic monitoring and treatment switching.

Prototype	Decision dimension	Details
A. Immune-excluded/ myeloid-dominant	State criteria	Low Arg/Cit; high ARG1/ARG2 or NOS2; CAF-ECM barrier; marginal $CD8^+$ T cells; strong polyamine uptake-efflux cycling
	Dominant bottleneck	Spatial exclusion; ARG-driven depletion; suppressive polyamine cloud
	Preferred sequence	Input/spatial repair → polyamine blockade → bypass-informed ferroptosis sensitization
	Example combinations	Arginase inhibition ± spatial repair; DFMO + AMXT1501; later FSP1/DHODH/BH4-informed sensitization
	Minimal PD readouts	Arg/Cit; ARG1/ARG2/NOS2; $CD8^+$ entry; acetylated polyamines; cDC1/cross-presentation; FSP1/DHODH/BH4
	Switch triggers	No improvement in $CD8^+$ entry or DC processing → return to repair; bypass buffering increases → add bypass-targeted sensitization; myeloid rewriting increases → reduce output pressure
B. Immune-inflamed/ IFN-γ-executable	State criteria	Active IFN-γ/cytotoxic programs; preserved DC processing; SLC7A11/system x_c^- vulnerability; variable bypass buffering
	Dominant bottleneck	Hidden anti-ferroptotic buffering limits immune-driven amplification
	Preferred sequence	ICB-driven immune activation →system x_c^- weakening → bypass-stratified ferroptosis sensitization
	Example combinations	ICB; ICB + system x_c^-pressure; ICB + DHODH/FSP1/BH4-informed sensitization
	Minimal PD readouts	IFN-γ signature; CXCL9/CXCL10; SLC7A11/GPX4; FSP1/ DHODH/BH4; DC maturation
	Switch triggers	DC processing declines → use pulsed/windowed pressure; bypass buffering increases → shift to bypass dismantling; inflamed-to-excluded drift → follow Prototype A
C. ASS1-low/ arginine-dependent	State criteria	Low or defective ASS1; exogenous arginine dependence; sensitivity to arginine deprivation; risk of ASS1 re-expression
	Dominant bottleneck	Dependency window, but excessive deprivation may impair immune execution
	Preferred sequence	ADI-PEG20 induction → immune/substrate support → output sensitization after state reassessment
	Example combinations	ADI-PEG20/pegargiminase ± chemotherapy or ICB; later ferroptosis sensitization according to buffering status
	Minimal PD readouts	ASS1 expression/methylation; Arg/Cit; immune phenotype; IFN-γ axis; FSP1/DHODH/BH4
	Switch triggers	ASS1 re-expression → stop relying on deprivation; IFN-γ or DC function declines → reduce deprivation intensity; state shifts to excluded/inflamed → follow A or B
D. Immune-desert/ priming-deficient	State criteria	Low cDC1; weak antigen presentation; poor $CD8^+$ infiltration; absent IFN-γ/cytotoxic programs
	Dominant bottleneck	No effective immune receiver for ferroptotic output
	Preferred sequence	Build immune priming/processing → repair access if needed → introduce output amplification only after immune conversion
	Example combinations	DC-priming strategies; antigen-presentation enhancement; spatial repair; later ICB or ferroptosis sensitization according to new state
	Minimal PD readouts	cDC1 markers; MHC-I/TAP1/2/B2M; DC maturation; $CD8^+$ infiltration; myeloid suppression index

Table II. Continued.

Prototype	Decision dimension	Details
	Switch triggers	Priming fails → avoid output amplification; desert-to-excluded transition → follow A; desert-to-inflamed transition → follow B

ADI-PEG20, pegylated arginine deiminase; AMXT1501, polyamine-transport inhibitor; Arg, arginine; ARG1, arginase 1; ARG2, arginase 2; ASS1, argininosuccinate synthase 1; B2M, beta-2-microglobulin; BH4, tetrahydrobiopterin; CAF, cancer-associated fibroblast; CD8, cluster of differentiation 8; cDC1, conventional type 1 dendritic cell; Cit, citrulline; CXCL9, C-X-C motif chemokine ligand 9; CXCL10, C-X-C motif chemokine ligand 10; DC, dendritic cell; DFMO, difluoromethylornithine; DHODH, dihydroorotate dehydrogenase; ECM, extracellular matrix; FSP1, ferroptosis suppressor protein 1; GPX4, glutathione peroxidase 4; ICB, immune checkpoint blockade; IFN-γ, interferon-γ; MHC-I, major histocompatibility complex class I; NOS2, nitric oxide synthase 2; PD, pharmacodynamic; SLC7A11, solute carrier family 7 member 11; system x_c^-, cystine/glutamate antiporter; TAP1/2, transporter associated with antigen processing 1/2.

Prototype A: Immune-excluded, myeloid-dominant tumors with high ARG activity and a strong polyamine cloud. In this prototype, the dominant bottleneck is typically not initially located at the Output layer. Instead, therapeutic failure arises from poor spatial accessibility and high inhibitory feedback gain, which prevents ferroptosis output from combining with effective immune amplification. Thus, Prototype A represents a state that should prioritize early repair rather than immediate Output-layer amplification. A more appropriate sequence is to first restore Input-layer arginine availability and improve spatial accessibility, then disrupt the State-layer polyamine-cloud cycle. Only after immune entry and processing capacity improve should ferroptosis amplification be introduced, with additional sensitization guided by the status of anti-ferroptosis bypass defenses (98,101,106).

Prototype A is not intended as a universal definition for all immune-excluded tumors but rather as a working model for those where the primary failure point lies in the decoupling of death output from the immune circuit. A minimal pharmacodynamic panel should include arginine/citrulline (Arg/Cit) dynamics, ARG/NOS-axis activity, spatial redistribution of $CD8^+$ T cells from the tumor margin to the parenchyma, acetylated-polyamine ratios or other polyamine-flux surrogates, DC/cDC1 processing capacity and anti-ferroptosis bypass markers. If immune entry and processing capacity fail to improve, or if bypass buffering becomes dominant, treatment should shift to further spatial repair, suppressive-network dismantling or schedule adjustments, rather than premature ferroptosis amplification. Operational assignments for Prototype A should simultaneously require evidence of immune-exclusion patterns and myeloid/ARG-polyamine dominance. High expression of a single marker, such as ARG1 or cluster of differentiation 163, is insufficient. The immune-exclusion components should be demonstrated by the preferential localization of $CD8^+$ T cells at the invasive margin rather than their distribution within the tumor parenchyma, while suppressive-network dominance should be supported by concordant myeloid-cell enrichment, ARG/NOS activity and arginine/polyamine metabolic measurements.

Prototype B: Immune-inflamed tumors with an executable IFN-γ axis. In this prototype, the system already incorporates baseline positive-feedback potential, with the dominant bottleneck typically shifting from spatial inaccessibility to hidden anti-ferroptotic buffering. Despite the presence of immune activity, Output-layer amplification may still be limited by bypass defenses such as FSP1, DHODH and GCH1/BH4, which elevate the effective ferroptosis threshold (74,85). Therefore, Prototype B represents a state where immune activity should first be written into the threshold. ICB may activate $CD8^+$ T cells and IFN-γ signaling, suppress the system x_c^--GSH antioxidant axis and weaken the tumor-cell buffering capacity. Subsequently, ferroptosis sensitization should be adjusted based on the status of bypass defenses, further amplifying the existing immune-ferroptosis window.

The key implication is that therapeutic failure in immune-inflamed tumors does not necessarily indicate insufficient immune activation. Rather, it may reflect persistent hidden buffering that prevents immune-derived oxidative pressure from translating into executable ferroptosis output. Therefore, the minimal pharmacodynamic panel should include IFN-γ/cytotoxicity signatures, system x_c^--related indicators, anti-ferroptotic bypass markers including FSP1, DHODH and GCH1/BH4 and dendritic-cell processing capacity. If dendritic-cell function declines, treatment should shift from continuous pressure to a windowed or pulsed schedule. If bypass buffering increases, the strategy should shift from single-axis amplification to bypass dismantling. If the immune-inflammatory state drifts toward immune exclusion, the therapeutic logic should revert to the Prototype A sequence: repair first, amplify later (4,94). Operational assignments for Prototype B should require intratumoral effector-cell infiltration, combined with active IFN-γ and antigen-presentation programs. Markers such as FSP1, DHODH, GCH1 and SLC7A11/GPX4 should be used to define the dominant ferroptosis-buffering mechanism, rather than establishing the immune-inflamed phenotype itself.

Prototype C: ASS1-low auxotrophic tumors with exogenous arginine dependence. The core feature of this prototype is a strong Input-layer dependency window arising from limited endogenous arginine-replenishment capacity. In ASS1-low tumors, arginine-deprivation strategies such as pegylated arginine deiminase (ADI-PEG20) can induce acute Input crisis and show clinical activity in specific disease contexts (107). However, the dominant bottleneck

is dual. Arginine deprivation may inhibit tumor growth but may also further reduce local arginine availability below the threshold required for effector T-cell function, thereby weakening immune execution. Additionally, therapeutic pressure may induce ASS1 re-expression or alternative replenishment programs, leading to state-coordinate drift (108,109).

Therefore, Prototype C should not be interpreted as a linear scenario where continuous arginine deprivation alone is sufficient. Rather, arginine deprivation should be viewed as an initiating Input-layer perturbation that must be combined with immune support, pharmacodynamic monitoring and adaptive sequences. A practical sequence could be formulated as follows: ADI-PEG20-based Input perturbation, followed by immune-supportive or threshold-protective interventions and then Output-layer ferroptosis amplification guided by trigger capacity and bypass-buffering status. If ASS1 re-expression, enhanced arginine-replenishment capacity, or simultaneous declines in IFN-γ signaling and dendritic-cell processing capacity are observed, treatment should shift to reducing perturbation intensity, window interventions or reclassifying to Prototype A or B pathways, rather than further intensifying arginine-deprivation pressure (110,111). Prototype C should not be assigned solely based on reduced ASS1 expression. Functional arginine auxotrophy should be confirmed by impaired growth under arginine-depleted conditions, failure of citrulline supplementation to fully restore proliferation and/or restoration of resistance following ASS1 re-expression. Sensitivity to ADI-PEG20 may provide additional functional readouts but should be interpreted alongside treatment-induced ASS1 re-expression and alternative arginine-replenishment pathways.

Prototype D: Immune-desert tumors with deficient processing capacity. In this prototype, the main bottleneck is initially not the threshold for ferroptosis, but rather the lack of an established Feedback circuit. When immune-initiating gain and dendritic-cell processing capacity are deficient, the amplified ferroptotic outputs cannot be effectively captured and presented to trigger adaptive immune amplification. Instead, it may promote the recruitment of myeloid cells and negative-feedback remodeling (112). Therefore, Prototype D represents a state where Feedback-layer construction should precede Output-layer amplification. The priority is to establish immune priming and processing capacity, while repairing spatial accessibility when necessary. Amplification of ferroptosis should only be introduced after the system transitions from an immune-desert state to a manageable immune state.

The key implication is that not all cold tumors are suitable for intensive ferroptosis induction. When immune-processing capacity is absent, Output-layer enhancement may lack an effective immune receiver and may instead feed negative feedback. Thus, the minimal pharmacodynamic panel should initially prioritize cDC1 abundance, dendritic-cell maturation, cross-presentation modules, and spatial immune-phenotype transition, rather than ferroptosis markers alone. Once the immune-desert state shifts toward an immune-excluded or immune-inflamed phenotype, subsequent sequencing should follow the logic of Prototype A or Prototype B, respectively (4,113,114).

Operational assignment and reference standards. Operational assignment should follow a two-step procedure. First, tumor-cell arginine dependency should be assessed to determine whether there is a functional ASS1-low nutritional deficiency coverage. Second, the immune-spatial state should be classified as Prototype A, B or D based on the distribution of $CD8^+$ T cells and cDC1s, IFN-γ and antigen-presentation activity, and the dominance of myeloid/ARG-polyamine suppression. Tumors that do not satisfy a single dominant pattern should be reported as mixed or transitional states, rather than being forcibly categorized into one category.

Reference standards should be specific to the detection. The spatial immune phenotype should be prioritized for assessment using multiplex immunohistochemistry, multiplex immunofluorescence or spatial transcriptomics. The arginine and polyamine status should be supported by targeted metabolomics, rather than solely relying on transcriptional expression. The ferroptosis-buffering state should be assessed using combined expression and activity-related indicators, as the abundance of GPX4, FSP1 or DHODH does not necessarily reflect pathway flux. Functional auxotrophy should be confirmed through arginine-deprivation assays, citrulline-rescue experiments or ASS1-restoration experiments. These measurements should be calibrated against disease-specific control tissues, independent validation cohorts or prospectively defined assay thresholds.

The proposed criteria are intended to serve as candidate operational standards rather than clinically validated diagnostic thresholds. Their reproducibility, relative weight and predictive value need to be validated in spatially annotated patient cohorts, *in vitro* tumor models and prospective pharmacodynamic studies.

Summary: The four prototypes provide a sequential decision scaffold. These four prototypes are not intended to support a universal therapeutic combination or clinically validated diagnostic classification. Instead, they emphasize that a rational combination therapy should first identify the main failure points in the Input-State-Output-Feedback system, and then match the therapeutic sequence, combination structure and amplification timing accordingly. Prototype assignment should be based on composite molecular, metabolic, spatial and functional evidence rather than on individual markers.

Prototypes A, B and D represent dominant immune-spatial states, whereas Prototype C represents an orthogonal metabolic dependency that may coexist with any of the three immune-spatial states. Therefore, these prototypes should be understood as rule-level and potential composite representations within a state-matching decision framework. Their reproducibility, clinical relevance thresholds and predictive value need to be validated through spatially resolved, longitudinal and pharmacodynamic studies.

State drift, switch triggers and dynamic reassessment. Therapeutic resistance can be defined as system-level drift between distinct tumor-immune states, rendering the original therapeutic sequence mismatched with the dominant bottleneck. Therefore, switch triggers should be incorporated into dynamic decision rules and the Input-State-Output-Feedback coordinates should be reassessed longitudinally during the treatment process.

Input drift includes ASS1 re-expression, altered arginine uptake or enhanced ARG/NOS activity, indicating

Table III. Representative pharmacological agents and investigational compounds targeting the Input-State-Output-Feedback framework.

Layer and molecular target	Representative agents or drug classes	Principal pharmacological action	Development stage	Key limitations
Input: ARG1/ARG2	Numidargistat/CB 1158; OATD-02	Inhibit arginase activity and preserve extracellular L-arginine availability for antitumor immune cells	Preclinical and early clinical investigation	Limited activity may occur in spatially excluded tumors or in the presence of compensatory myeloid suppressive pathways
Input: ASS1-low arginine dependency	ADI-PEG20/ pegargiminase	Enzymatically deplete extracellular arginine in arginine-auxotrophic tumors	Clinical investigation	May impair effector T-cell function and select for ASS1 re-expression or alternative arginine-replenishment pathways
State: Polyamine synthesis and transport	Eflornithine/ DFMO; DFMO plus AMXT1501	Inhibit ODC1-dependent polyamine synthesis and block compensatory extracellular polyamine uptake	Preclinical and early clinical investigation	Uptake compensation, metabolic adaptation and normal-tissue exposure may limit efficacy
Output: system x_c^--GSH-GPX4 axis	Sulfasalazine and other system x_c^- inhibitors; experimental direct GPX4 inhibitors	Restrict cystine-dependent GSH synthesis or directly impair phospholipid-hydroperoxide detoxification	Drug repurposing and preclinical investigation	Non-selective systemic GPX4 inhibition may cause severe normal-tissue toxicity, including renal injury. Direct GPX4 inhibitors remain preclinical and require tumor-selective delivery, intermittent dosing and renal safety monitoring
Output: FSP1-CoQ10 defense	iFSP1 and other experimental FSP1 inhibitors	Disrupt GPX4-independent CoQ10 reduction and plasma-membrane radical trapping	Preclinical	Lack of clinically validated inhibitors, tumor-selective delivery systems and established pharmacodynamic biomarkers
Output: DHODH-CoQ defense	Brequinar and other DHODH inhibitors	Inhibit mitochondrial CoQ reduction and weaken mitochondrial ferroptosis buffering	Preclinical ferroptosis investigation	Activity depends on GPX4 abundance, mitochondrial dependence and compensatory extra mitochondrial defenses
Feedback: PD-1/ PD-L1 immune-checkpoint axis	Anti-PD-1 and anti-PD-L1 antibodies	Restore $CD8^+$ T-cell activity and IFN-γ-dependent suppression of tumor antioxidant defenses	Clinically established drug class	Limited efficacy in immune-excluded, immune-desert or dendritic-cell-processing-deficient tumors

The table is restricted to representative targets for which identifiable pharmacological agents or investigational compounds are available. Mechanistic targets without sufficiently established pharmacological agents, including GCH1-BH4 modulation, polyamine-catabolic oxidative triggering and ESCRT-III/iPLA2β-mediated terminal defenses, are discussed in the main text but are not included in this drug-centered summary. ADI-PEG20, pegylated arginine deiminase; ARG1, arginase 1; ARG2, arginase 2; ASS1, argininosuccinate synthase 1; BH4, tetrahydrobiopterin; CD8, cluster of differentiation 8; CoQ, coenzyme Q; CoQ10, coenzyme Q10; DHODH, dihydroorotate dehydrogenase; DFMO, difluoromethylornithine; ESCRT-III, endosomal sorting complex required for transport III; FSP1, ferroptosis suppressor protein 1; GCH1, GTP cyclohydrolase 1; GPX4, glutathione peroxidase 4; GSH, glutathione; IFN-γ, interferon-γ; iPLA2β, calcium-independent phospholipase A2 beta; ODC1, ornithine decarboxylase 1; PD-1, programmed cell death protein 1; PD-L1, programmed death-ligand 1; system x_c^-, cystine/glutamate antiporter.

a restoration of the tumor-cell replenishment capacity or progression toward a myeloid-dominant arginine-restricted state. State drift includes increased ODC1/AMD1-driven synthesis, SAT1/PAOX/SMOX-associated catabolic flux or restabilization of polyamine uptake-efflux cycling. Output drift is reflected as an increase in ferroptosis buffering, such as SLC7A11/GPX4, FSP1, DHODH or GCH1/BH4, or insufficient triggering capacity involving ACSL4/LPCAT3, ALOX15 or TFRC/NCOA4. Feedback drift includes the loss of IFN-γ/cytotoxicity signatures, impaired dendritic-cell processing, reduced antigen presentation or a transition towards immune exclusion or immune desert.

These drift triggers should define the switching routes in Table II. Dynamic reassessment helps distinguish true therapeutic resistance from state mismatch and determines whether the next step should be Input-layer repair, State-layer disruption, Output-layer amplification or Feedback-layer restoration.

Safety boundaries for ferroptosis-directed combinations. Given that GPX4 and its associated anti-lipid-peroxidation networks are essential for normal tissue homeostasis, ferroptosis-targeted combination therapies require both precise state matching and strict safety boundaries. The guiding principle should be to stratify first and then intensify. Prior to Output-layer amplification, the core ferroptosis-defense axis and parallel bypass systems, including system x_c^--GSH-GPX4 axis, FSP1-CoQ10, DHODH-CoQ and GCH1/BH4, should be evaluated to avoid ineffective or harmful exposure in tumors that do not rely on the target buffering axis.

Safety should also influence therapeutic sequencing. Input-layer interventions may provide upstream leverage but require monitoring for systemic metabolic effects and unintended T-cell suppression. State-layer polyamine blockade may disrupt suppressive buffering, but long-term exposure should be carefully evaluated because polyamines support normal tissue renewal and immune-cell function. Thus, ferroptosis-directed combinations should use stepwise escalation guided by pharmacodynamic evidence of tumor vulnerability, bypass-buffering status and preserved immune competence.

7. Future perspectives and conclusions

To make this state-matching immunopharmacological framework practically applicable in translation, the key challenge lies not in further expanding the list of node-level mechanisms but in transforming the proposed Input-State-Output-Feedback coordinates into clinically accessible, reproducible and updateable readout systems. Thus, in the present review, the framework was presented as a conceptual yet testable working model. Its value lies not in replacing disease-specific evidence, but in providing a unified language to define what should be monitored, how therapeutic states should be validated, how sequential trials should be designed and when treatment routes should be switched.

At the monitoring level, future work should establish a minimal variable set that supports dynamic state reassessment rather than relying on single static indicators. At the Input layer, monitoring may include Arg/Cit dynamics, ASS1 status, ARG/NOS-axis activity and spatial flux surrogates. At the State layer, priority should be given to surrogate readouts of polyamine flux, such as acetylated-polyamine ratios, paired synthetic and catabolic signatures and spatial-omics constraints. At the Output layer, ACSL4/LPCAT3, iron-metabolism surrogates and buffering markers including GPX4, FSP1 and DHODH should be interpreted jointly. At the Feedback layer, longitudinal panels should assess dendritic-cell processing capacity, spatial accessibility and myeloid-mediated suppressive remodeling. A useful monitoring system should not be defined by the number of variables included, but by whether it can determine, during treatment, whether the tumor system has undergone a state transition.

Spatial heterogeneity should be assessed by combining tissue-resolved mapping with repeatable whole-tumor imaging. Spatial transcriptomics and multiplex immunostaining of pretreatment or on-treatment biopsies can identify CAF-rich and ECM-dense regions, their proximity to functional vasculature, local myeloid accumulation and exclusion of $CD8^+$ T cells. However, these tissue-based methods provide spatial snapshots and become longitudinal only when applied to serial, image-guided biopsies (115). Dynamic contrast-enhanced magnetic resonance imaging can non-invasively quantify regional perfusion and vascular permeability, including parameters such as K^trans, while serial ^18F-fluoromisonidazole positron emission tomography/computed tomography can map and track hypoxic tumor subvolumes during treatment (116,117). Therefore, a practical clinical workflow would co-register imaging at baseline and during treatment, obtain biopsies from radiographically distinct regions when feasible, and combine these findings with spatial omics and circulating metabolite measurements. This multimodal strategy may distinguish persistent transport barriers from reversible metabolic states and determine whether interventions improve nutrient delivery and immune accessibility before ferroptosis amplification. Table III summarizes representative intervention leverage points classified according to the Input-State-Output-Feedback framework.

Acknowledgements

Not applicable.

Funding

The present study was supported by the Nantong Municipal Science and Technology Plan Project (grant no. MSZ2025012), the Nantong Natural Science Foundation (grant no. JC2025056), the Nantong Municipal Health Commission Directive Project-General Program (grant no. MS2025037), the Health Development Promotion Project (grant no. KM-20250805-01) and the Nantong University Clinical Medicine Special Funding Project (grant no. 2024JY040).

Availability of data and materials

Not applicable.

Authors' contributions

XD and YH contributed to conceptualization, literature review, manuscript drafting and figure preparation. JS contributed to literature organization and manuscript revision. HZ and JL supervised the work, contributed to conceptual refinement and critically revised the manuscript. All authors read and approved the final manuscript. Data authentication is not applicable.

Ethics approval and consent to participate

Not applicable.

Patient consent for publication

Not applicable.

Competing interests

The authors declare that they have no competing interests.

Use of artificial intelligence tools

During the preparation of this work, artificial intelligence tools were used to improve the readability and language of the manuscript or to generate images, and subsequently, the authors revised and edited the content produced by the artificial intelligence tools as necessary, taking full responsibility for the ultimate content of the present manuscript. No generative AI tools were used to create scientific figures.

References

1. Canale FP, Basso C, Antonini G, Perotti M, Li N, Sokolovska A, Neumann J, James MJ, Geiger S, Jin W, *et al*: Metabolic modulation of tumours with engineered bacteria for immunotherapy. Nature 598: 662-666, 2021.
2. Zou Z, Cheng Q, Zhou J, Guo C, Hadjinicolaou AV, Salio M, Liang X, Yang C, Du Y, Yao W, *et al*: ATF4-SLC7A11-GSH axis mediates the acquisition of immunosuppressive properties by activated $CD4^+$ T cells in low arginine condition. Cell Rep 43: 113995, 2024.
3. Bi G, Liang J, Bian Y, Shan G, Huang Y, Lu T, Zhang H, Jin X, Chen Z, Zhao M, *et al*: Polyamine-mediated ferroptosis amplification acts as a targetable vulnerability in cancer. Nat Commun 15: 2461, 2024.
4. Wiernicki B, Maschalidi S, Pinney J, Adjemian S, Vanden Berghe T, Ravichandran KS and Vandenabeele P: Cancer cells dying from ferroptosis impede dendritic cell-mediated anti-tumor immunity. Nat Commun 13: 3676, 2022.
5. Catanzaro E, Demuynck R, Naessens F, Galluzzi L and Krysko DV: Immunogenicity of ferroptosis in cancer: A matter of context? Trends Cancer 10: 407-416, 2024.
6. Lim AR, Rathmell WK and Rathmell JC: The tumor microenvironment as a metabolic barrier to effector T cells and immunotherapy. Elife 9: e55185, 2020.
7. DePeaux K and Delgoffe GM: Metabolic barriers to cancer immunotherapy. Nat Rev Immunol 21: 785-797, 2021.
8. Matos A, Carvalho M, Bicho M and Ribeiro R: Arginine and arginases modulate metabolism, tumor microenvironment and prostate cancer progression. Nutrients 13: 4503, 2021.
9. Bai D, Zhou Y, Jing L, Guo C and Yang Q: Arginine metabolism in cancer biology and immunotherapy. Immune Netw 25: e30, 2025.
10. Missiaen R, Lesner NP and Simon MC: HIF: A master regulator of nutrient availability and metabolic cross-talk in the tumor microenvironment. EMBO J 42: e112067, 2023.
11. Wu Y, Chen Z, Chen X, Hu Y and Ma Y: Recent advances in the investigation of the regulatory network underlying reactive nitrogen species-mediated tumorigenesis: Molecular mechanisms and targeted therapeutic strategies. Redox Rep 30: 2564593, 2025.
12. Wetzel TJ, Erfan SC, Figueroa LD, Wheeler LM and Ananieva EA: Crosstalk between arginine, glutamine, and the branched chain amino acid metabolism in the tumor microenvironment. Front Oncol 13: 1186539, 2023.
13. Dunlap KN, Bender A, Bowles A, Bott AJ, Tay J, Grossmann AH, Rutter J and Ducker GS: SLC7A5 is required for cancer cell growth under arginine-limited conditions. Cell Rep 44: 115130, 2025.
14. Wu Y, Wu Y, Gao Z, Yu W, Zhang L and Zhou F: Revitalizing T cells: Breakthroughs and challenges in overcoming T cell exhaustion. Signal Transduct Target Ther 11: 2, 2026.
15. Grzybowski MM, Uçal Y, Muchowicz A, Rejczak T, Kikulska A, Głuchowska KM, Szostakowska-Rodzoś M, Zagożdżon A, Bausbacher T, Tkaczyk A, *et al*: Metabolomic reprogramming of the tumor microenvironment by dual arginase inhibitor OATD-02 boosts anticancer immunity. Sci Rep 15: 18741, 2025.
16. Engel K, Höhne W and Häberle J: Mutations and polymorphisms in the human argininosuccinate synthetase (ASS1) gene. Hum Mutat 30: 300-307, 2009.
17. Lim LQJ, Adler L, Hajaj E, Soria LR, Perry RBT, Darzi N, Brody R, Furth N, Lichtenstein M, Bab-Dinitz E, *et al*: ASS1 metabolically contributes to the nuclear and cytosolic p53-mediated DNA damage response. Nat Metab 6: 1294-1309, 2024.
18. Ding Q, Li R, Wang Q, Yu L and Zi F: A pan-cancer analysis of the role of argininosuccinate synthase 1 in human tumors. Front Oncol 13: 1049147, 2023.
19. Rabinovich S, Adler L, Yizhak K, Sarver A, Silberman A, Agron S, Stettner N, Sun Q, Brandis A, Helbling D, *et al*: Diversion of aspartate in ASS1-deficient tumours fosters de novo pyrimidine synthesis. Nature 527: 379-383, 2015.
20. Crump NT, Hadjinicolaou AV, Xia M, Walsby-Tickle J, Gileadi U, Chen JL, Setshedi M, Olsen LR, Lau IJ, Godfrey L, *et al*: Chromatin accessibility governs the differential response of cancer and T cells to arginine starvation. Cell Rep 35: 109101, 2021.
21. Gai X, Liu Y, Lan X, Chen L, Yuan T, Xu J, Li Y, Zheng Y, Yan Y, Yang L, *et al*: Oncogenic KRAS induces arginine auxotrophy and confers a therapeutic vulnerability to SLC7A1 inhibition in non-small cell lung cancer. Cancer Res 84: 1963-1977, 2024.
22. Raber PL, Thevenot P, Sierra R, Wyczechowska D, Halle D, Ramirez ME, Ochoa AC, Fletcher M, Velasco C, Wilk A, *et al*: Subpopulations of myeloid-derived suppressor cells impair T cell responses through independent nitric oxide-related pathways. Int J Cancer 134: 2853-2864, 2014.
23. Corzo CA, Condamine T, Lu L, Cotter MJ, Youn JI, Cheng P, Cho HI, Celis E, Quiceno DG, Padhya T, *et al*: HIF-1α regulates function and differentiation of myeloid-derived suppressor cells in the tumor microenvironment. J Exp Med 207: 2439-2453, 2010.
24. Menjivar RE, Nwosu ZC, Du W, Donahue KL, Hong HS, Espinoza C, Brown K, Velez-Delgado A, Yan W, Lima F, *et al*: Arginase 1 is a key driver of immune suppression in pancreatic cancer. Elife 12: e80721, 2023.
25. Rotondo R, Bertolotto M, Barisione G, Astigiano S, Mandruzzato S, Ottonello L, Dallegri F, Bronte V, Ferrini S and Barbieri O: Exocytosis of azurophil and arginase 1-containing granules by activated polymorphonuclear neutrophils is required to inhibit T lymphocyte proliferation. J Leukoc Biol 89: 721-727, 2011.
26. Martí I Líndez AA and Reith W: Arginine-dependent immune responses. Cell Mol Life Sci 78: 5303-5324, 2021.
27. Raynor JL and Chi H: Nutrients: Signal 4 in T cell immunity. J Exp Med 221: e20221839, 2024.
28. Sattiraju A, Kang S, Giotti B, Chen Z, Marallano VJ, Brusco C, Ramakrishnan A, Shen L, Tsankov AM, Hambardzumyan D, *et al*: Hypoxic niches attract and sequester tumor-associated macrophages and cytotoxic T cells and reprogram them for immunosuppression. Immunity 56: 1825-1843.e6, 2023.
29. Arpinati L, Carradori G and Scherz-Shouval R: CAF-induced physical constraints controlling T cell state and localization in solid tumours. Nat Rev Cancer 24: 676-693, 2024.
30. Pegg AE: Mammalian polyamine metabolism and function. IUBMB Life 61: 880-894, 2009.

31. Smirnova OA, Bartosch B, Zakirova NF, Kochetkov SN and Ivanov AV: Polyamine metabolism and oxidative protein folding in the ER as ROS-producing systems neglected in virology. Int J Mol Sci 19: 1219, 2018.
32. DeFelice BC and Fiehn O: Rapid LC-MS/MS quantification of cancer related acetylated polyamines in human biofluids. Talanta 196: 415-419, 2019.
33. Cerrada-Gimenez M, Häkkinen MR, Vepsäläinen J, Auriola S, Alhonen L and Keinänen TA: Polyamine flux analysis by determination of heavy isotope incorporation from 13C, 15N-enriched amino acids into polyamines by LC-MS/MS. Amino Acids 42: 451-460, 2012.
34. Thomas DD, Espey MG, Ridnour LA, Hofseth LJ, Mancardi D, Harris CC and Wink DA: Hypoxic inducible factor 1alpha, extracellular signal-regulated kinase, and p53 are regulated by distinct threshold concentrations of nitric oxide. Proc Natl Acad Sci USA 101: 8894-8899, 2004.
35. Kapralov AA, Yang Q, Dar HH, Tyurina YY, Anthonymuthu TS, Kim R, St Croix CM, Mikulska-Ruminska K, Liu B, Shrivastava IH, *et al*: Redox lipid reprogramming commands susceptibility of macrophages and microglia to ferroptotic death. Nat Chem Biol 16: 278-290, 2020.
36. Zhu L, Leng D, Guo Z, Zhao Y, Leung KT, Dai Y, Li J and Zhao Q: Self-catalyzed nitric oxide nanocomplexes induce ferroptosis for cancer immunotherapy. J Control Release 377: 524-539, 2025.
37. Cognet G and Muir A: Identifying metabolic limitations in the tumor microenvironment. Sci Adv 10: eadq7305, 2024.
38. Henke E, Nandigama R and Ergün S: Extracellular matrix in the tumor microenvironment and its impact on cancer therapy. Front Mol Biosci 6: 160, 2020.
39. Jain RK: Normalization of tumor vasculature: An emerging concept in antiangiogenic therapy. Science 307: 58-62, 2005.
40. Apiz Saab JJ, Dzierozynski LN, Jonker PB, AminiTabrizi R, Shah H, Menjivar RE, Scott AJ, Nwosu ZC, Zhu Z, Chen RN, *et al*: Pancreatic tumors exhibit myeloid-driven amino acid stress and upregulate arginine biosynthesis. Elife 12: e81289, 2023.
41. Babbar N and Casero RA Jr: Tumor necrosis factor-alpha increases reactive oxygen species by inducing spermine oxidase in human lung epithelial cells: A potential mechanism for inflammation-induced carcinogenesis. Cancer Res 66: 11125-11130, 2006.
42. Van den Bossche J, Lamers WH, Koehler ES, Geuns JMC, Alhonen L, Uimari A, Pirnes-Karhu S, Van Overmeire E, Morias Y, Brys L, *et al*: Pivotal advance: Arginase-1-independent polyamine production stimulates the expression of IL-4-induced alternatively activated macrophage markers while inhibiting LPS-induced expression of inflammatory genes. J Leukoc Biol 91: 685-699, 2012.
43. Puleston DJ, Baixauli F, Sanin DE, Edwards-Hicks J, Villa M, Kabat AM, Kamiński MM, Stanckzak M, Weiss HJ, Grzes KM, *et al*: Polyamine metabolism is a central determinant of helper T cell lineage fidelity. Cell 184: 4186-4202.e20, 2021.
44. Dixon SJ, Lemberg KM, Lamprecht MR, Skouta R, Zaitsev EM, Gleason CE, Patel DN, Bauer AJ, Cantley AM, Yang WS, *et al*: Ferroptosis: an iron-dependent form of nonapoptotic cell death. Cell 149: 1060-1072, 2012.
45. Doll S, Proneth B, Tyurina YY, Panzilius E, Kobayashi S, Ingold I, Irmler M, Beckers J, Aichler M, Walch A, *et al*: ACSL4 dictates ferroptosis sensitivity by shaping cellular lipid composition. Nat Chem Biol 13: 91-98, 2017.
46. Holbert CE, Cullen MT, Casero RA Jr and Stewart TM: Polyamines in cancer: Integrating organismal metabolism and antitumour immunity. Nat Rev Cancer 22: 467-480, 2022.
47. Miska J, Rashidi A, Lee-Chang C, Gao P, Lopez-Rosas A, Zhang P, Burga R, Castro B, Xiao T, Han Y, *et al*: Polyamines drive myeloid cell survival by buffering intracellular pH to promote immunosuppression in glioblastoma. Sci Adv 7: eabc8929, 2021.
48. Wu T, Yankovskaya V and McIntire WS: Cloning, sequencing, and heterologous expression of the murine peroxisomal flavoprotein, N1-acetylated polyamine oxidase. J Biol Chem 278: 20514-20525, 2003.
49. Pegg AE: Spermidine/spermine-N(1)-acetyltransferase: A key metabolic regulator. Am J Physiol Endocrinol Metab 294: E995-E1010, 2008.
50. Kramer DL, Diegelman P, Jell J, Vujcic S, Merali S and Porter CW: Polyamine acetylation modulates polyamine metabolic flux, a prelude to broader metabolic consequences. J Biol Chem 283: 4241-4251, 2008.
51. Kashiwagi K and Igarashi K: Molecular characteristics of toxicity of acrolein produced from spermine. Biomolecules 13: 298, 2023.
52. Uemura T, Takasaka T, Igarashi K and Ikegaya H: Spermine oxidase promotes bile canalicular lumen formation through acrolein production. Sci Rep 7: 14841, 2017.
53. Narayanan SP, Shosha E and Palani CD: Spermine oxidase: A promising therapeutic target for neurodegeneration in diabetic retinopathy. Pharmacol Res 147: 104299, 2019.
54. Diaz E, Adhikary S, Tepper AWJW, Riley D, Ortiz-Meoz R, Krosky D, Buyck C, Lamenca CM, Llaveria J, Fang L, *et al*: Structure of human spermine oxidase in complex with a highly selective allosteric inhibitor. Commun Biol 5: 787, 2022.
55. Yang H, Tai F, Wang T, Zheng X, Ge C, Qin Y and Fu H: Hydrogen peroxide and iron ions can modulate lipid peroxidation, apoptosis, and the cell cycle, but do not have a significant effect on DNA double-strand break. Biochem Biophys Res Commun 651: 121-126, 2023.
56. Ou Y, Wang SJ, Li D, Chu B and Gu W: Activation of SAT1 engages polyamine metabolism with p53-mediated ferroptotic responses. Proc Natl Acad Sci USA 113: E6806-E6812, 2016.
57. Bian Y, Shan G, Bi G, Xu Z, Liang J, Yan Y, Guo W, Sui Q, Yi Y, Shi H, *et al*: Targeting polyamine metabolism and ferroptosis enhances the efficacy of KRAS-targeted therapy depending on KEAP1 status. Nat Commun 16: 9923, 2025.
58. Hibino S, Eto S, Hangai S, Endo K, Ashitani S, Sugaya M, Osawa T, Soga T, Taniguchi T and Yanai H: Tumor cell-derived spermidine is an oncometabolite that suppresses TCR clustering for intratumoral CD8$^+$ T cell activation. Proc Natl Acad Sci USA 120: e2305245120, 2023.
59. Li G, Ding H, Yu X, Meng Y, Li J, Guo Q, Zhou H and Shen N: Spermidine suppresses inflammatory DC function by activating the FOXO3 pathway and counteracts autoimmunity. iScience 23: 100807, 2020.
60. Yang H, Zhang X, Zhang S, Yang Y, Chen Y, Jiang Y, Lu Q, Liu L, Lao M, Du W, *et al*: Targeting spermine metabolism to overcome immunotherapy resistance in pancreatic cancer. Nat Commun 16: 7827, 2025.
61. Ru Q, Li Y, Chen L, Wu Y, Min J and Wang F: Iron homeostasis and ferroptosis in human diseases: Mechanisms and therapeutic prospects. Signal Transduct Target Ther 9: 271, 2024.
62. Wenzel SE, Tyurina YY, Zhao J, St Croix CM, Dar HH, Mao G, Tyurin VA, Anthonymuthu TS, Kapralov AA, Amoscato AA, *et al*: PEBP1 wardens ferroptosis by enabling lipoxygenase generation of lipid death signals. Cell 171: 628-641.e26, 2017.
63. Kagan VE, Mao G, Qu F, Angeli JPF, Doll S, Croix CS, Dar HH, Liu B, Tyurin VA, Ritov VB, *et al*: Oxidized arachidonic and adrenic PEs navigate cells to ferroptosis. Nat Chem Biol 13: 81-90, 2017.
64. Viswanathan VS, Ryan MJ, Dhruv HD, Gill S, Eichhoff OM, Seashore-Ludlow B, Kaffenberger SD, Eaton JK, Shimada K, Aguirre AJ, *et al*: Dependency of a therapy-resistant state of cancer cells on a lipid peroxidase pathway. Nature 547: 453-457, 2017.
65. Jain S, Zhang X, Khandelwal PJ, Saunders AJ, Cummings BS and Oelkers P: Characterization of human lysophospholipid acyltransferase 3. J Lipid Res 50: 1563-1570, 2009.
66. Dixon SJ, Winter GE, Musavi LS, Lee ED, Snijder B, Rebsamen M, Superti-Furga G and Stockwell BR: Human haploid cell genetics reveals roles for lipid metabolism genes in nonapoptotic cell death. ACS Chem Biol 10: 1604-1609, 2015.
67. Zou Y, Li H, Graham ET, Deik AA, Eaton JK, Wang W, Sandoval-Gomez G, Clish CB, Doench JG and Schreiber SL: Cytochrome P450 oxidoreductase contributes to phospholipid peroxidation in ferroptosis. Nat Chem Biol 16: 302-309, 2020.
68. Hassannia B, Vandenabeele P and Vanden Berghe T: Targeting ferroptosis to iron out cancer. Cancer Cell 35: 830-849, 2019.
69. Lin Z, Chen H, Ke Y, Xiao H, Li C, Wu Z, Gao H, Huang N, Lu L, Sun P and Bian Y: Iron overload in the tumor microenvironment induces CD8$^+$ T cell ferroptosis and dysfunction. Nat Commun 17: 6754, 2026.
70. Yang WS and Stockwell BR: Ferroptosis: Death by lipid peroxidation. Trends Cell Biol 26: 165-176, 2016.
71. Friedmann Angeli JP, Schneider M, Proneth B, Tyurina YY, Tyurin VA, Hammond VJ, Herbach N, Aichler M, Walch A, Eggenhofer E, *et al*: Inactivation of the ferroptosis regulator Gpx4 triggers acute renal failure in mice. Nat Cell Biol 16: 1180-1191, 2014.

72. Hou DY, Cheng DB, Zhang NY, Wang ZJ, Hu XJ, Li X, Lv MY, Li XP, Jian LR, Ma JP, *et al*: In vivo assembly enhanced binding effect augments tumor specific ferroptosis therapy. Nat Commun 15: 454, 2024.
73. Doll S, Freitas FP, Shah R, Aldrovandi M, da Silva MC, Ingold I, Goya Grocin A, Xavier da Silva TN, Panzilius E, Scheel CH, *et al*: FSP1 is a glutathione-independent ferroptosis suppressor. Nature 575: 693-698, 2019.
74. Bersuker K, Hendricks JM, Li Z, Magtanong L, Ford B, Tang PH, Roberts MA, Tong B, Maimone TJ, Zoncu R, *et al*: The CoQ oxidoreductase FSP1 acts parallel to GPX4 to inhibit ferroptosis. Nature 575: 688-692, 2019.
75. Mishima E, Ito J, Wu Z, Nakamura T, Wahida A, Doll S, Tonnus W, Nepachalovich P, Eggenhofer E, Aldrovandi M, *et al*: A non-canonical vitamin K cycle is a potent ferroptosis suppressor. Nature 608: 778-783, 2022.
76. Mao C, Liu X, Zhang Y, Lei G, Yan Y, Lee H, Koppula P, Wu S, Zhuang L, Fang B, *et al*: DHODH-mediated ferroptosis defence is a targetable vulnerability in cancer. Nature 593: 586-590, 2021.
77. Kraft VAN, Bezjian CT, Pfeiffer S, Ringelstetter L, Müller C, Zandkarimi F, Merl-Pham J, Bao X, Anastasov N, Kössl J, *et al*: GTP cyclohydrolase 1/tetrahydrobiopterin counteract ferroptosis through lipid remodeling. ACS Cent Sci 6: 41-53, 2020.
78. Dai E, Meng L, Kang R, Wang X and Tang D: ESCRT-III-dependent membrane repair blocks ferroptosis. Biochem Biophys Res Commun 522: 415-421, 2020.
79. Pedrera L, Espiritu RA, Ros U, Weber J, Schmitt A, Stroh J, Hailfinger S, von Karstedt S and García-Sáez AJ: Ferroptotic pores induce Ca^{2+} fluxes and ESCRT-III activation to modulate cell death kinetics. Cell Death Differ 28: 1644-1657, 2021.
80. Chen D, Chu B, Yang X, Liu Z, Jin Y, Kon N, Rabadan R, Jiang X, Stockwell BR and Gu W: iPLA2β-mediated lipid detoxification controls p53-driven ferroptosis independent of GPX4. Nat Commun 12: 3644, 2021.
81. Sun WY, Tyurin VA, Mikulska-Ruminska K, Shrivastava IH, Anthonymuthu TS, Zhai YJ, Pan MH, Gong HB, Lu DH, Sun J, *et al*: Phospholipase $iPLA_2\beta$ averts ferroptosis by eliminating a redox lipid death signal. Nat Chem Biol 17: 465-476, 2021.
82. Koppula P, Lei G, Zhang Y, Yan Y, Mao C, Kondiparthi L, Shi J, Liu X, Horbath A, Das M, *et al*: A targetable CoQ-FSP1 axis drives ferroptosis- and radiation-resistance in KEAP1 inactive lung cancers. Nat Commun 13: 2206, 2022.
83. Han X, Wang D, Yang L, Wang N, Shen J, Wang J, Zhang L, Chen L, Gao S, Zong WX and Wang Y: Activation of polyamine catabolism promotes glutamine metabolism and creates a targetable vulnerability in lung cancer. Proc Natl Acad Sci USA 121: e2319429121, 2024.
84. Efimova I, Catanzaro E, Van der Meeren L, Turubanova VD, Hammad H, Mishchenko TA, Vedunova MV, Fimognari C, Bachert C, Coppieters F, *et al*: Vaccination with early ferroptotic cancer cells induces efficient antitumor immunity. J Immunother Cancer 8: e001369, 2020.
85. Wang W, Green M, Choi JE, Gijón M, Kennedy PD, Johnson JK, Liao P, Lang X, Kryczek I, Sell A, *et al*: $CD8^+$ T cells regulate tumour ferroptosis during cancer immunotherapy. Nature 569: 270-274, 2019.
86. Cramer SL, Saha A, Liu J, Tadi S, Tiziani S, Yan W, Triplett K, Lamb C, Alters SE, Rowlinson S, *et al*: Systemic depletion of L-cyst(e)ine with cyst(e)inase increases reactive oxygen species and suppresses tumor growth. Nat Med 23: 120-127, 2017.
87. Feig C, Jones JO, Kraman M, Wells RJB, Deonarine A, Chan DS, Connell CM, Roberts EW, Zhao Q, Caballero OL, *et al*: Targeting CXCL12 from FAP-expressing carcinoma-associated fibroblasts synergizes with anti-PD-L1 immunotherapy in pancreatic cancer. Proc Natl Acad Sci USA 110: 20212-20217, 2013.
88. Shen J, Choi YL, Lee T, Kim H, Chae YK, Dulken BW, Bogdan S, Huang M, Fisher GA, Park S, *et al*: Inflamed immune phenotype predicts favorable clinical outcomes of immune checkpoint inhibitor therapy across multiple cancer types. J Immunother Cancer 12: e008339, 2024.
89. Mellman I, Chen DS, Powles T and Turley SJ: The cancer-immunity cycle: Indication, genotype, and immunotype. Immunity 56: 2188-2205, 2023.
90. Silva Barcelos EC, Ricciuti D, Mondanelli G and Gargaro M: Rewriting the dendritic cell code in cancer-from subset identity to immunotherapeutic design. FEBS Lett 599: 2060-2083, 2025.
91. Gilmour BC, Corthay A and Øynebråten I: High production of IL-12 by human dendritic cells stimulated with combinations of pattern-recognition receptor agonists. NPJ Vaccines 9: 83, 2024.
92. López-Albaitero A, Mailliard R, Hackman T, Filho PAA, Wang X, Gooding W, Ferrone S, Kalinski P and Ferris RL: Maturation pathways of dendritic cells determine TAP1 and TAP2 levels and cross-presenting function. J Immunother 32: 465-473, 2009.
93. Ayers M, Lunceford J, Nebozhyn M, Murphy E, Loboda A, Kaufman DR, Albright A, Cheng JD, Kang SP, Shankaran V, *et al*: IFN-γ-related mRNA profile predicts clinical response to PD-1 blockade. J Clin Invest 127: 2930-2940, 2017.
94. Grasso CS, Tsoi J, Onyshchenko M, Abril-Rodriguez G, Ross-Macdonald P, Wind-Rotolo M, Champhekar A, Medina E, Torrejon DY, Shin DS, *et al*: Conserved interferon-γ signaling drives clinical response to immune checkpoint blockade therapy in melanoma. Cancer Cell 38: 500-515.e3, 2020.
95. Tiwari A, Oravecz T, Dillon LA, Italiano A, Audoly L, Fridman WH and Clifton GT: Towards a consensus definition of immune exclusion in cancer. Front Immunol 14: 1084887, 2023.
96. Joyce JA and Fearon DT: T cell exclusion, immune privilege, and the tumor microenvironment. Science 348: 74-80, 2015.
97. Gobbini E, Hubert M, Doffin AC, Eberhardt A, Hermet L, Li D, Duplouye P, Ghamry-Barrin S, Berthet J, Benboubker V, *et al*: The spatial organization of cDC1 with $CD8^+$ T cells is critical for the response to immune checkpoint inhibitors in patients with melanoma. Cancer Immunol Res 13: 517-526, 2025.
98. Mariathasan S, Turley SJ, Nickles D, Castiglioni A, Yuen K, Wang Y, Kadel EE III, Koeppen H, Astarita JL, Cubas R, *et al*: TGFβ attenuates tumour response to PD-L1 blockade by contributing to exclusion of T cells. Nature 554: 544-548, 2018.
99. Dai E, Han L, Liu J, Xie Y, Kroemer G, Klionsky DJ, Zeh HJ, Kang R, Wang J and Tang D: Autophagy-dependent ferroptosis drives tumor-associated macrophage polarization via release and uptake of oncogenic KRAS protein. Autophagy 16: 2069-2083, 2020.
100. Liu ZY, Wu CY, Wu RQ, Wang JC, Huang CX, Wang XY, Zhang Y, Zheng L, Chen Y, Lao XM, *et al*: Efflux of N1-acetylspermidine from hepatoma fosters macrophage-mediated immune suppression to dampen immunotherapeutic efficacy. Immunity 58: 1572-1585.e10, 2025.
101. Hayes CS, Shicora AC, Keough MP, Snook AE, Burns MR and Gilmour SK: Polyamine-blocking therapy reverses immunosuppression in the tumor microenvironment. Cancer Immunol Res 2: 274-285, 2014.
102. Murray Stewart T, Dunston TT, Woster PM and Casero RA Jr: Polyamine catabolism and oxidative damage. J Biol Chem 293: 18736-18745, 2018.
103. Tcyganov EN, Sanseviero E, Marvel D, Beer T, Tang HY, Hembach P, Speicher DW, Zhang Q, Donthireddy LR, Mostafa A, *et al*: Peroxynitrite in the tumor microenvironment changes the profile of antigens allowing escape from cancer immunotherapy. Cancer Cell 40: 1173-1189.e6, 2022.
104. Srivastava MK, Sinha P, Clements VK, Rodriguez P and Ostrand-Rosenberg S: Myeloid-derived suppressor cells inhibit T cell activation by depleting cystine and cysteine. Cancer Res 70: 68-77, 2010.
105. Nagaraj S, Gupta K, Pisarev V, Kinarsky L, Sherman S, Kang L, Herber DL, Schneck J and Gabrilovich DI: Altered recognition of antigen is a mechanism of CD8+ T cell tolerance in cancer. Nat Med 13: 828-835, 2007.
106. Rodriguez PC, Quiceno DG, Zabaleta J, Ortiz B, Zea AH, Piazuelo MB, Delgado A, Correa P, Brayer J, Sotomayor EM, *et al*: Arginase I production in the tumor microenvironment by mature myeloid cells inhibits T-cell receptor expression and antigen-specific T-cell responses. Cancer Res 64: 5839-5849, 2004.
107. Szlosarek PW, Steele JP, Nolan L, Gilligan D, Taylor P, Spicer J, Lind M, Mitra S, Shamash J, Phillips MM, *et al*: Arginine deprivation with pegylated arginine deiminase in patients with argininosuccinate synthase 1-deficient malignant pleural mesothelioma: A randomized clinical trial. JAMA Oncol 3: 58-66, 2017.
108. Rodriguez PC, Zea AH, Culotta KS, Zabaleta J, Ochoa JB and Ochoa AC: Regulation of T cell receptor CD3zeta chain expression by L-arginine. J Biol Chem 277: 21123-21129, 2002.
109. Chang KY, Chiang NJ, Wu SY, Yen CJ, Chen SH, Yeh YM, Li CF, Feng X, Wu K, Johnston A, *et al*: Phase 1b study of pegylated arginine deiminase (ADI-PEG 20) plus pembrolizumab in advanced solid cancers. Oncoimmunology 10: 1943253, 2021.

110. Zea AH, Rodriguez PC, Culotta KS, Hernandez CP, DeSalvo J, Ochoa JB, Park HJ, Zabaleta J and Ochoa AC: L-Arginine modulates CD3zeta expression and T cell function in activated human T lymphocytes. Cell Immunol 232: 21-31, 2004.
111. Phillips MM, Pavlyk I, Allen M, Ghazaly E, Cutts R, Carpentier J, Berry JS, Nattress C, Feng S, Hallden G, *et al*: A role for macrophages under cytokine control in mediating resistance to ADI-PEG20 (pegargiminase) in ASS1-deficient mesothelioma. Pharmacol Rep 75: 570-584, 2023.
112. Fuertes MB, Kacha AK, Kline J, Woo SR, Kranz DM, Murphy KM and Gajewski TF: Host type I IFN signals are required for antitumor CD8+ T cell responses through CD8{alpha}+ dendritic cells. J Exp Med 208: 2005-2016, 2011.
113. Conche C, Finkelmeier F, Pešić M, Nicolas AM, Böttger TW, Kennel KB, Denk D, Ceteci F, Mohs K, Engel E, *et al*: Combining ferroptosis induction with MDSC blockade renders primary tumours and metastases in liver sensitive to immune checkpoint blockade. Gut 72: 1774-1782, 2023.
114. Sánchez-Paulete AR, Teijeira Á, Quetglas JI, Rodríguez-Ruiz ME, Sánchez-Arráez Á, Labiano S, Etxeberria I, Azpilikueta A, Bolaños E, Ballesteros-Briones MC, *et al*: Intratumoral immunotherapy with XCL1 and sFlt3L encoded in recombinant Semliki Forest virus-derived vectors fosters dendritic cell-mediated T-cell cross-priming. Cancer Res 78: 6643-6654, 2018.
115. Wu SZ, Al-Eryani G, Roden DL, Junankar S, Harvey K, Andersson A, Thennavan A, Wang C, Torpy JR, Bartonicek N, *et al*: A single-cell and spatially resolved atlas of human breast cancers. Nat Genet 53: 1334-1347, 2021.
116. Little RA, Barjat H, Hare JI, Jenner M, Watson Y, Cheung S, Holliday K, Zhang W, O'Connor JPB, Barry ST, *et al*: Evaluation of dynamic contrast-enhanced MRI biomarkers for stratified cancer medicine: How do permeability and perfusion vary between human tumours? Magn Reson Imaging 46: 98-105, 2018.
117. Tachibana I, Nishimura Y, Shibata T, Kanamori S, Nakamatsu K, Koike R, Nishikawa T, Ishikawa K, Tamura M and Hosono M: A prospective clinical trial of tumor hypoxia imaging with 18F-fluoromisonidazole positron emission tomography and computed tomography (F-MISO PET/CT) before and during radiation therapy. J Radiat Res 54: 1078-1084, 2013.